DISSERTATION

DEVELOPMENTS IN AUTOMATED ELECTROCHEMICAL BIOSENSORS TO IMPROVE POINT OF CARE DIAGNOSTICS

Submitted by

Melissa Schenkel

Department of Chemistry

In partial fulfillment of requirements

For the Degree of Doctor of Philosophy

Colorado State University

Fort Collins, Colorado

Fall 2022

Doctoral Committee:

Advisor: Alan Kennan

Charles Henry
Christopher Snow
Eric Ross

ABSTRACT

DEVELOPMENTS IN AUTOMATED ELECTROCHEMICAL BIOSENSORS TO IMPROVE POINT OF CARE DIAGNOSTICS

The onset of the COVID-19 pandemic brought public attention to the pre-existing need for developments in diagnostics, especially at the point of care. While traditional techniques, like PCR, can be highly sensitive and specific, they are also time consuming, expensive, and require trained personnel in a laboratory setting and expensive equipment. The need for point of care diagnostic options was made evident in early 2020 when laboratories could not keep up with the high demand for COVID-19 testing. Lateral flow assays (LFAs) like home pregnancy tests offer a platform that is inexpensive, easy to use, and can produce results rapidly at the point of care. Unfortunately, LFAs usually exhibit poor sensitivity and limits of detection compared to traditional techniques. Electrochemical biosensors can provide a diagnostic platform that is quick, cost effective, accurate, highly sensitive, and quantitative. While electrochemical biosensors incorporated in lateral flow devices have improved sensitivity, they typically require complex fabrication techniques, and the nitrocellulose platform can limit electrochemical performance. The Henry group has recently reported a new class of capillary-driven fluidic devices using alternating layers of patterned polyethylene terephthalate (PET) films and double-sided adhesives (DSA) that can control flow for sequential delivery of reagents.

This work presents recent developments in automated electrochemical biosensors to improve point of care diagnostics. The incorporation of electrochemical biosensors with the aforementioned novel fluidic devices provides a diagnostic platform that has the potential to

achieve the sensitivity and selectivity rivaling that of traditional techniques while maintaining the ease of use of an LFA.

Chapter 2 of this dissertation first presents an electrochemical immunosensor for detection of SARS-CoV-2 N-protein. This sensor was then adapted and optimized for compatibility in a fluidic device. This included optimizing ease of functionalization with manufacturing-friendly techniques, exploring different buffers for assay steps, and optimizing assay components Ultimately, these studies led to automated, concentration-dependent detection of SARS-CoV-2 N-protein upon a single sample addition step.

Chapter 3 of this dissertation presents a novel device design that improved flow rates, decreased device malfunctions, and incorporated commercial electrodes. This device was developed for measurements of C-reactive protein, a common biomarker of inflammation. Utilizing gold electrodes has the potential for more sensitive detection compared to carbon electrodes and aptamers as biological recognition elements provides many advantages as well. While work on this project is still underway, the results presented herein demonstrate the ability of this novel diagnostic device to be adapted for various analytes.

Future work includes continued assay and device optimization, with the intent for multiplexed detection of multiple analytes. Overall, the work presented here provides a novel platform for point of care diagnostics and demonstrates its application to two different analytes.

TABLE OF CONTENTS

ABSTRACT……ii
Chapter 1: Introduction……1
Electrochemical Biosensors……..……3
Electrochemical Transducers……4
Biological Recognition Elements……..5
Analytes……6
Fluidic Devices and Electrochemical Biosensors at the Point of Care……..7
Capillary Driven Immunoassay Device……9
Contributions……...10
References……12
Chapter 2: Development of a Covid-19 immunosensor and assay adaptions for incorporating into automated electrochemical capillary-driven immunoassay device……17
Summary……..17
Introduction……..18
Materials and Methods……20
Results and Discussion……26
Conclusions and Future Directions..……42
References……....44
Chapter 3: Electrochemical aptamer-based assay for measurement of CRP in automated fluidic device……47
Summary……..47
Introduction……..47
Materials and Methods……51
Results and Discussion……55
Conclusions and Future Directions……..66
References……67
Chapter 4: Conclusions and Future Directions……..71
Future Directions……73
References……75

Chapter 1: Introduction

In late December 2019, the novel coronavirus SARS-CoV-2 emerged in Wuhan City, China. The months that followed saw rapid spreading of the virus across the globe, overwhelmed hospitals unable to care for patients, and many lives lost. It was declared a global pandemic on March 11, 2020, and as of July 2022 has claimed over 6 million lives. As society pivoted to adjust to the pandemic, laboratories became overwhelmed with diagnostic tests, and unable to keep up with the growing demand. This shed light on the drastic need for developments in diagnostic technologies, especially at the point of need.

Luckily, there was already research underway that was able to be adapted to address the crisis at hand. This, along with loosened restrictions on approval processes, enabled rapid developments in diagnostics. **Figure 1.1** presents a condensed timeline highlighting the rapid developments in Covid-19 diagnostics that were achieved in 2020. The SARS-CoV-2 genome was released on January 12, 2020, and less than one month later, on February 4th, the first PCR test had received emergency use authorization (EUA) from the FDA.[1] PCR tests use a technique from which they get their name known formally as reverse transcriptase polymerase chain reaction (RT-PCR). This is a highly sensitive laboratory assay that enzymatically amplifies a defined nucleic acid sequence.[2] It has been used in research and laboratory settings to measure mRNA,[2] detect solid tumors,[3] and to diagnose tuberculosis,[4] prostate cancer,[5] Covid-19,[6] and so much more. Despite the sensitivity and versatility of this assay, it is not a good option as a point of care diagnostic as it requires expensive laboratory equipment, trained personnel, and can take several hours to complete. This was made evident by the lack of tests available in the early stages of the pandemic.

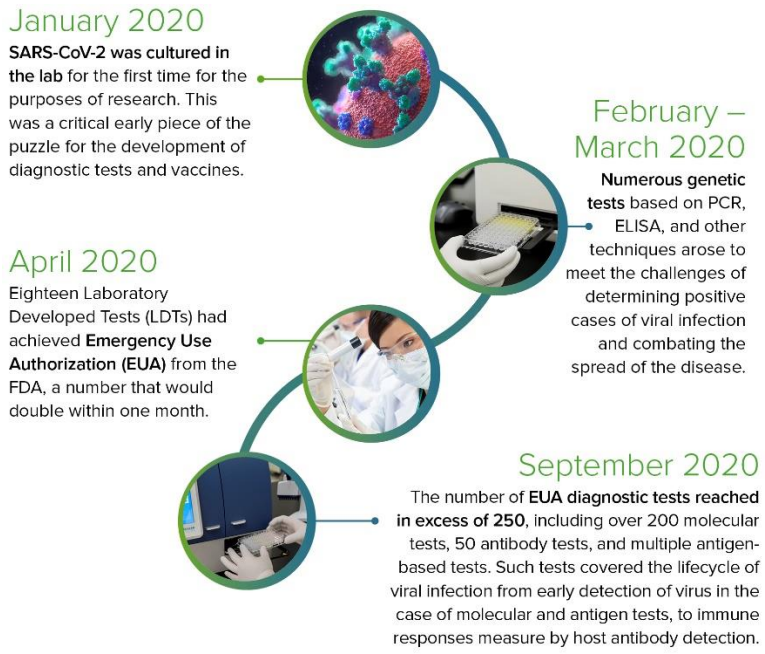

Figure 1.1: Condensed timeline highlighting the rapid developments in diagnositic options for Covid-19 that emerged throughout 2020. This image was published by Molecular Devices on their website.[7]

The disadvantages of PCR were not previously unknown. Therefore, the development of diagnostic options for Covid-19 followed a similar, albeit accelerated, path to diagnostics for other viruses, proteins, etc. On March 3rd, the first antibody test was made available, followed shortly by the first antigen test on May 9th. These tests utilize a technique known as an immunoassay, which uses an analyte-specific antibody or antigen to act as a recognition element and bind with high affinity and specificity to the given analyte. Prior to the pandemic, these tests were available in commercial kits for analytes like C-reactive protein,[8] pesticide analysis,[9] Influenza A and B,[10] measles virus,[11] and many more. Despite providing an alternative to PCR, these assays still need to be done in a laboratory, with expensive equipment and trained personnel.

The first lateral flow assay (LFA) was launched in 1984 to serve as an at-home pregnancy test.[12] This type of test relies on the same antibody/antigen binding principle as an immunoassay, but have been developed to enable single-step detection at the point of care. These typically function

by capillary action through a nitrocellulose strip to deliver sample and reagents dried within the device across a detection zone. They usually include a test and control line, resulting in the appearance of a single line for a negative sample and a double line for a positive sample.[13] Unsurprisingly, the first LFA test for Covid-19 followed shortly after the immunoassays.[14] Unfortunately, these devices are usually underperforming in sensitivity and limits of detection (LODs).[15, 16]

Many efforts have been made to improve the performance of LFAs by incorporating electrochemical transducers.[17] An electrochemical transducer, represented in **Figure 1.2,** is responsible for transforming analytical information originating from the electrochemical analyte-electrode interaction into a measurable electrical signal.[18] These electrochemical LFA devices have been developed to detect a wide variety of analytes ranging from, but not limited to, hormones like testosterone,[19] to large proteins like troponin[20] and albumin,[21] viruses like H1N1.[22] Before these transducers can be incorporated in LFA devices, the electrochemical sensing mechanism must first be developed and optimized for the analyte of interest. This requires the development of electrochemical biosensors.

Electrochemical biosensors:

Electrochemical biosensors have been instrumental in advancing point-of-care (POC) testing due to their ability to provide the high sensitivity inherent in electrochemical transducers with the high specificity of biological recognition processes. **Figure 1.2** provides a general schematic of an electrochemical biosensor.

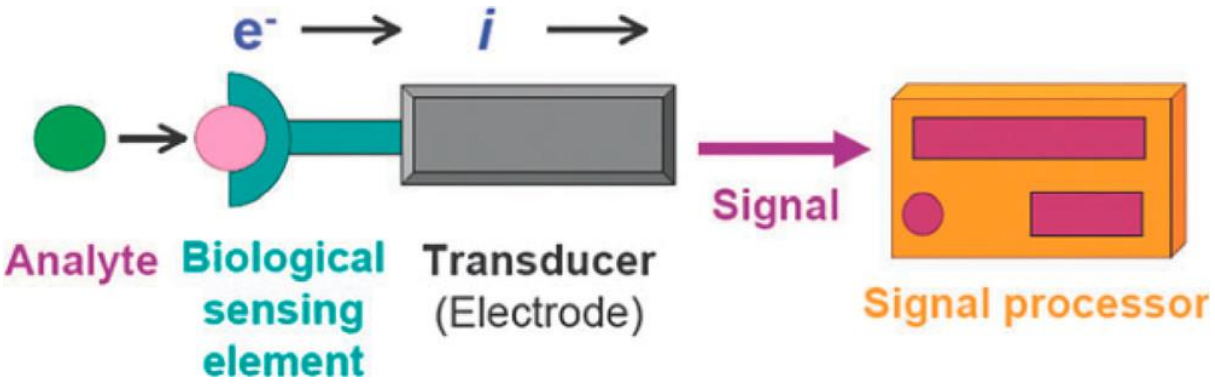

Figure 1.2: This figure was initially published by Ronkainen *et al.* in Chemical Society Reviews. It presents a schematic of an electrochemical biosensor.[23] Necessary components of a biosensor include a biological sensing element that binds with high specificity and selectivity to the given analyte, an electrochemical transducer to convert the electrochemical response of the binding event to a measurable signal, and a signal processor for reading and measuring the signal.

Electrochemical Transducers

Electrochemical biosensors, a sub-class of biosensors, utilize a conductive electrode material as the transducer. This is an appealing component, especially in the context of POC biosensing, because it has the potential to combine the high sensitivity of electrochemical transducers with the specificity of biological recognition processes while being low-cost, easy to produce, easy to use, and more portable compared to other transducers.[23] Typical electrode materials include solid precious metals, liquid metals, carbon materials, or semiconductors.[24] Most biosensors incorporate gold, platinum, or carbon electrodes, although the development of new electrode materials is a growing area of research.[25-27]

Gold is a favorable electrode material as it exhibits excellent electron transfer kinetics, relatively good stability, and is chemically inert and biocompatible.[28-30] Further, thiol-gold interactions are well characterized, making for simple functionalization of the electrode with thiol-terminated biological recognition elements.[31-33] Despite the advantages of gold, there are more cost-effective

alternatives. Carbon materials have been gaining interest and are attractive due to their low cost, wide potential window, relatively inert electrochemistry, and electrocatalytic activity.[34] Screen-printing electrodes allows for easy miniaturization and manufacturing, usually resulting in lower costs.[35] Applications using both gold and carbon screen-printed electrodes will be discussed in this dissertation.

Biological Recognition elements

The most commonly used recognition element for affinity based sensors are antibodies that bind with high sensitivity and specificity to a given antigen.[36] The popularity of this technique was largely sparked by the work of Kohler and Milstein in the 1970's which presented the ability to use cell clones to produce a monoclonal antibody of choice.[37] Since then, there have been numerous reports of biosensors developed relying on the binding of antibodies with antigens to produce a measurable signal.[38-40] The largest advantages of antibodies as a biosensing recognition element include the high sensitivity and specificity with which they bind to a target analyte, the ability to continuously produce a monoclonal antibody of choice, and the widespread research that has already been done to develop antibody-based assays. Despite the advantages and advancements that have been made, there are several drawbacks to antibody-based sensors. Some of these include the laborious and expensive production of antibodies, batch-to-batch variation causing the need for re-optimizations, limitations to physiological conditions and analytes that are tolerated by animals, temperature sensitivity, and limited shelf life due to irreversible denaturation.[41]

To overcome some of these challenges, a more recent area of research gaining popularity in affinity-based biosensing is the use of aptamers as the recognition element.[41] Aptamers are a class of molecules that emerged in the 1990s.[42, 43] They are single-stranded nucleic acids that fold into

specific 3D structures and selectively bind to a target analyte. Aptamers have many advantages that counter the disadvantages of antibodies. They can be chemically synthesized, reducing the opportunity for batch-to-batch variation, they can detect analytes that would be toxic or incompatible with mammalian cells, they are more stable than proteins, and can be used repeatedly without losing their binding capacity. Further, due to their smaller size, aptamers may achieve higher density for immobilization on a biosensor.[44] The use of aptamers as a recognition element with be further explored in Chapter 3 of this report for the detection of C-reactive protein (CRP).

Analytes

The first, and perhaps most well-known, electrochemical biosensor was presented in the early 1960's as an enzyme electrode with immobilized glucose oxidase used to measure glucose levels in human blood. This technology hit the market in 1975, enabling point-of-care glucose monitoring for people with diabetes.[45] Similar devices have been developed to monitor the freshness of fish meat through the detection of xanthine using an electrode with immobilized xanthine oxidase,[46-48] and to measure lactate in sports medicine applications and in milk using enzymes like lactate dehydrogenase and lactate oxidase.[49, 50] While enzymatic sensors enable easy, direct detection of analytes, it is limited in applications to analytes that have a corresponding specific enzyme.

Affinity-based biosensors are another class of electrochemical biosensors that instead rely on strong binding of biological molecules like antibodies, nucleic acids, and membrane receptors with a complementary analyte.[23, 51] Immunosensors are the most common examples of this. They use an antibody as the recognition element and have been developed for detection of a wide range of molecules including bacteria like *E. coli*[52, 53] and *Salmonella,*[54, 55] hormones like testosterone[56] and progesterone,[57] cancer biomarkers,[58] and so many more.[59] The work presented in chapter 2 of this

dissertation focuses on the development of an electrochemical immunosensor for detection of Covid-19.

Fluidic devices and electrochemical biosensors at the point of care

While electrochemical biosensors can provide a detection mechanism that is quick, cost effective, accurate, highly sensitive, and easily quantitative, many of these techniques still require trained personnel to perform the assay. [60] As mentioned before, lateral flow assays (LFAs) are an alternative option commonly used for diagnostics at the point-of-care. The most common example of this is a home pregnancy test, but LFAs have been developed for detection of a wide range of clinically relevant analytes.[61]

LFAs are ideal for point of care diagnostics because they are inexpensive, can be used by an untrained user outside of a laboratory setting, and give a readout in minutes. Generally, the addition of a sample induces capillary action through a porous membrane to deliver the sample and reagents dried within the device to the test and control lines, producing a colorimetric signal of two lines for a positive sample and one line for a negative sample.[13] Despite the benefits of the simplicity of these devices, they typically suffer from poor sensitivity and limits of detection compared to more sophisticated laboratory techniques like ELISA,[16] and results are not typically quantitative. In some cases, like pregnancy tests, there is little need for quantitative results. However, quantitative readouts can be useful in applications like measuring HIV viral load before treatment or monitoring levels of C-reactive protein in response to anti-inflammatory medication.[62]

Electrochemical detection coupled with the simplicity and ease of use of an LFA offers a platform to provide more sensitive and quantitative readouts without the complicated assay procedures and expensive instrumentation. Further, miniaturization through the development of thick film

electrode techniques like screen-printing has enabled large-scale production of electrochemical devices at affordable prices.[62] Current disadvantages of electrochemical LFAs include complicated and expensive chip fabrications compared to traditional LFA strips, additional reagents and procedures are required for some assays, and electrochemical detection should be performed in solution phase.[63]

Microfluidic, and other flow devices are appealing, especially in clinical applications, due to the low sample-volumes required. They also eliminate the nitrocellulose platform of LFAs which can cause variable flow patterns, and difficulty releasing labels from conjugate pad, which can hinder reproducibility, sensitivity, and detection limits.[64] These hollow-channel devices have been developed to perform complicated laboratory techniques like rt-PCR, rt-LAMP, nested PCR, nucleic acid hybridization, ELISA, and fluorescence based assays.[65] These devices provide platforms that can control reactions, separations, delivery of reagents, and detections with high sensitivity, faster readouts, and lower cost compared to the traditional techniques.[66] In 2008, Liu *et al.* incorporated microelectrodes into a conventional flow-focusing microfluidic device to achieve detection and characterization of aqueous droplets.[67] Other notable studies incorporating electrochemical transducers in microfluidic devices include devices for cell analysis,[68] cancer diagnosis,[69] PCR platforms,[70] and multiplexed DNA detection.[71] Tang *et al.* developed an electrochemical microfluidic immunosensor for multiplexed detection of 4 tumor markers.[72] Despite the advancements and wide array of applications, the need for external pumps and the multiple user steps provide obstacles at the point of care.

Capillary driven devices provide a pump-free platform that can drive flow without the need for laboratory equipment.[73] Taking advantage of pump-free capillary action provided by paper, the Henry group recently developed a new class of fluidic devices using alternating layers of

polyethylene terephthalate (PET) films and double-sided adhesives (DSA) to create hollow channels with a paper pump inserted in the outlet channel to drive flow and demonstrated its utility for rapid mixing[74] and flow control.[75]

Capillary-driven immunoassay device

Using the newly developed fluidic platform to address the Covid-19 pandemic, a disposable, fluidic ELISA system for COVID-19 serology testing was created. This enabled the detection of SARS-CoV-2 antibodies with the sensitivity of an ELISA while maintaining the ease of use of an LFA. This was accomplished by creating fluidic channels with patterned, alternating PET films and double-sided adhesive. Once the sample was added, the fluid would wick through the channels toward a cellulose waste pad, driven by capillary flow, and sequentially deliver reagents dried within the device. The sequential reagent delivery served to automate the steps of a sandwich ELISA and yielded the traditional double-line readout for a positive sample and a single line for a negative sample.[76]

While this traditional readout is attractive due to the lack of instrumentation needed, it is not easily quantifiable and can be subjective to the user's interpretation especially at low concentrations when the line may appear faint and distorted. To overcome these drawbacks, another study incorporated a screen-printed electrode system just before the cellulose pump to take the place of the nitrocellulose readout strip. This new system was compatible with near field communication (NFC) potentiostats and could measure the electrochemical signal of the substrate turnover and report a quantitative result to a smart-phone.[77]

Contributions

While the ability to monitor previous exposure to COVID-19 is important from an epidemiological standpoint, it is not useful as a diagnostic tool. The work presented in Chapter 2 of this presentation is a continuation of this work. First, an electrochemical immunosensor was developed and optimized using stencil-printed carbon electrodes for detection of SARS-CoV-2 N-protein. Moving forward, the assay was adapted for screen-printed carbon electrodes, which could later be incorporated into a capillary-driven fluidic device for automated reagent delivery to complete the assay. Ultimately, this work resulted in two publications, the first can be found in *Analytical Chemistry* and presents the electrochemical detection of SARS-CoV-2 in Nasopharyngeal samples. The second publication has been accepted to *ACS Measurement Science Au* and describes the electrochemical capillary-driven immunoassay for detection of SARS-CoV-2.

Chapter 3 presents an electrochemical biosensor for measurement of C-reactive protein (CRP), a common biomarker of inflammation. CRP levels in saliva may be correlated to levels in human serum, with much lower concentrations found in saliva.[78-81] Detection in saliva is desirable since it is a non-invasive sample. To address the need for a highly sensitive and quantitative detection, commercial screen-printed gold electrodes were used for this study with a CRP-specific aptamer as a recognition element. After developing the assay, the electrochemical biosensor was incorporated into a novel capillary-driven fluidic device designed to improve upon previous work. The new fluidic device simplified fabrication as it was compatible with commercial electrodes. Further, it was designed to prevent device malfunctions observed in previous studies and increase flow rate, resulting in faster results compared to the electrochemical capillary-driven fluidic device for Covid-19 diagnosis. This project required more optimizations and experiments before publication.

Future work, discussed further in Chapter 4, aims to optimize the assay and fluidic device for CRP detection, and evaluated compatibility of the device using saliva samples. Going forward, this technology can continue to be developed for new and emerging analytes. Multiplexing the fluidic devices to enable simultaneous detection of different analytes would be extremely useful from a clinical diagnostic standpoint.

References

1. CDC Museum COVID-19 Timeline. https://www.cdc.gov/museum/timeline/covid19.html (accessed 7/20/2022).
2. Bustin, S. A., Absolute quantification of mRNA using real-time reverse transcription polymerase chain reaction assays. *Journal of molecular endocrinology* **2000,** *25* (2), 169-193.
3. Raj, G. V.; Moreno, J. G.; Gomella, L. G., Utilization of polymerase chain reaction technology in the detection of solid tumors. *Cancer: Interdisciplinary International Journal of the American Cancer Society* **1998,** *82* (8), 1419-1442.
4. Babafemi, E. O.; Cherian, B. P.; Banting, L.; Mills, G. A.; Ngianga, K., Effectiveness of real-time polymerase chain reaction assay for the detection of Mycobacterium tuberculosis in pathological samples: a systematic review and meta-analysis. *Systematic reviews* **2017,** *6* (1), 1-16.
5. Olsson, C. A.; de Vries, G. M.; Buttyan, R.; Katz, A. E., Reverse transcriptase-polymerase chain reaction assays for prostate cancer. *Urologic Clinics of North America* **1997,** *24* (2), 367-378.
6. Motley, M. P.; Bennett-Guerrero, E.; Fries, B. C.; Spitzer, E. D., Review of viral testing (polymerase chain reaction) and antibody/serology testing for severe acute respiratory syndrome-coronavirus-2 for the intensivist. *Critical care explorations* **2020,** *2* (6).
7. COVID-19 Timeline: Diagnostics, Vaccines, and Therapeutic Antibody Development. **2022**.
8. Morishita, Y.; Iinuma, Y.; Nakashima, N., A consideration on discrepancy of results obtained between commercial CRP measurement kits. *Rinsho byori. The Japanese Journal of Clinical Pathology* **2000,** *48* (8), 746-751.
9. Gabaldón, J. A.; Maquieira, A.; Puchades, R., Current trends in immunoassay-based kits for pesticide analysis. *Critical reviews in food science and nutrition* **1999,** *39* (6), 519-538.
10. Weinberg, A.; Walker, M. L., Evaluation of three immunoassay kits for rapid detection of influenza virus A and B. *Clinical and Vaccine Immunology* **2005,** *12* (3), 367-370.
11. Ratnam, S.; Gadag, V.; West, R.; Burris, J.; Oates, E.; Stead, F.; Bouilianne, N., Comparison of commercial enzyme immunoassay kits with plaque reduction neutralization test for detection of measles virus antibody. *Journal of clinical microbiology* **1995,** *33* (4), 811-815.
12. Mak, W. C.; Beni, V.; Turner, A. P., Lateral-flow technology: From visual to instrumental. *TrAC Trends in Analytical Chemistry* **2016,** *79*, 297-305.
13. Posthuma-Trumpie, G. A.; Korf, J.; van Amerongen, A., Lateral flow (immuno) assay: its strengths, weaknesses, opportunities and threats. A literature survey. *Analytical and bioanalytical chemistry* **2009,** *393* (2), 569-582.
14. Grant, B. D.; Anderson, C. E.; Williford, J. R.; Alonzo, L. F.; Glukhova, V. A.; Boyle, D. S.; Weigl, B. H.; Nichols, K. P., SARS-CoV-2 coronavirus nucleocapsid antigen-detecting half-strip lateral flow assay toward the development of point of care tests using commercially available reagents. *Analytical chemistry* **2020,** *92* (16), 11305-11309.
15. Mahmoudinobar, F.; Britton, D.; Montclare, J. K., Protein-based lateral flow assays for COVID-19 detection. *Protein Engineering, Design and Selection* **2021,** *34*.
16. Ong, D. S.; De Man, S.; Lindeboom, F. A.; Koeleman, J. G., Comparison of diagnostic accuracies of rapid serological tests and ELISA to molecular diagnostics in patients with suspected coronavirus disease 2019 presenting to the hospital. *Clinical Microbiology and Infection* **2020,** *26* (8), 1094. E7-1094. E10.

17. Cheng, J.; Yang, G.; Guo, J.; Liu, S.; Guo, J., Integrated electrochemical lateral flow immunoassays (eLFIAs): recent advances. *Analyst* **2022,** *147* (4), 554-570.
18. Ota, K.-i.; Kreysa, G.; Savinell, R. F., *Encyclopedia of applied electrochemistry*. Springer New York: 2014.
19. Inoue, K.; Ferrante, P.; Hirano, Y.; Yasukawa, T.; Shiku, H.; Matsue, T., A competitive immunochromatographic assay for testosterone based on electrochemical detection. *Talanta* **2007,** *73* (5), 886-892.
20. Akanda, M. R.; Joung, H.-A.; Tamilavan, V.; Park, S.; Kim, S.; Hyun, M. H.; Kim, M.-G.; Yang, H., An interference-free and rapid electrochemical lateral-flow immunoassay for one-step ultrasensitive detection with serum. *Analyst* **2014,** *139* (6), 1420-1425.
21. Yasukawa, T.; Kiba, Y.; Mizutani, F., A dual electrochemical sensor based on a test-strip assay for the quantitative determination of albumin and creatinine. *Analytical Sciences* **2015,** *31* (7), 583-589.
22. Bhardwaj, J.; Sharma, A.; Jang, J., Vertical flow-based paper immunosensor for rapid electrochemical and colorimetric detection of influenza virus using a different pore size sample pad. *Biosensors and Bioelectronics* **2019,** *126*, 36-43.
23. Ronkainen, N. J.; Halsall, H. B.; Heineman, W. R., Electrochemical biosensors. *Chemical Society Reviews* **2010,** *39* (5), 1747-1763.
24. Bard, A. J.; Faulkner, L. R.; White, H. S., *Electrochemical methods: fundamentals and applications*. John Wiley & Sons: 2022.
25. Otero, F.; Magner, E., Biosensors—recent advances and future challenges in electrode materials. *Sensors* **2020,** *20* (12), 3561.
26. Kumar, A.; Sharma, S.; Pandey, L. M.; Chandra, P., Nanoengineered material based biosensing electrodes for enzymatic biofuel cells applications. *Materials Science for Energy Technologies* **2018,** *1* (1), 38-48.
27. Ispas, C.; Njagi, J.; Cates, M.; Andreescu, S., Electrochemical studies of ceria as electrode material for sensing and biosensing applications. *Journal of the Electrochemical Society* **2008,** *155* (8), F169.
28. Koç, Y.; Moralı, U.; Erol, S.; Avci, H., Electrochemical investigation of gold based screen printed electrodes: an application for a seafood toxin detection. *Electroanalysis* **2021,** *33* (4), 1033-1048.
29. Gandouzi, I.; Tertis, M.; Cernat, A.; Bakhrouf, A.; Coros, M.; Pruneanu, S.; Cristea, C., Sensitive detection of pyoverdine with an electrochemical sensor based on electrochemically generated graphene functionalized with gold nanoparticles. *Bioelectrochemistry* **2018,** *120*, 94-103.
30. Tallapragada, S. D.; Layek, K.; Mukherjee, R.; Mistry, K. K.; Ghosh, M., Development of screen-printed electrode based immunosensor for the detection of HER2 antigen in human serum samples. *Bioelectrochemistry* **2017,** *118*, 25-30.
31. Jasmin, J.-P.; Cannizzo, C.; Dumas, E.; Chaussé, A., Fabrication and characterization of all-covalent nanocomposite functionalized screen-printed voltammetric sensors. *Electrochimica Acta* **2014,** *133*, 467-474.
32. Shin, S. R.; Kilic, T.; Zhang, Y. S.; Avci, H.; Hu, N.; Kim, D.; Branco, C.; Aleman, J.; Massa, S.; Silvestri, A., Label-Free and Regenerative Electrochemical Microfluidic Biosensors for Continual Monitoring of Cell Secretomes. *Advanced Science* **2017,** *4* (5), 1600522.

33. Ravalli, A.; Dos Santos, G. P.; Ferroni, M.; Faglia, G.; Yamanaka, H.; Marrazza, G., New label free CA125 detection based on gold nanostructured screen-printed electrode. *Sensors and Actuators B: Chemical* **2013,** *179*, 194-200.
34. McCreery, R. L., Advanced carbon electrode materials for molecular electrochemistry. *Chemical reviews* **2008,** *108* (7), 2646-2687.
35. Davis, J.; Vaughan, D. H.; Cardosi, M. F., Elements of biosensor construction. *Enzyme and microbial technology* **1995,** *17* (12), 1030-1035.
36. Chambers, J. P.; Arulanandam, B. P.; Matta, L. L.; Weis, A.; Valdes, J. J., Biosensor recognition elements. *Current issues in molecular biology* **2008,** *10* (1-2), 1-12.
37. Köhler, G.; Milstein, C., Continuous cultures of fused cells secreting antibody of predefined specificity. *Nature* **1975,** *256* (5517), 495-497.
38. Sharma, S.; Byrne, H.; O'Kennedy, R. J., Antibodies and antibody-derived analytical biosensors. *Essays in biochemistry* **2016,** *60* (1), 9-18.
39. Vashist, S. K.; Lam, E.; Hrapovic, S.; Male, K. B.; Luong, J. H., Immobilization of antibodies and enzymes on 3-aminopropyltriethoxysilane-functionalized bioanalytical platforms for biosensors and diagnostics. *Chemical reviews* **2014,** *114* (21), 11083-11130.
40. Vidal, J. C.; Bonel, L.; Ezquerra, A.; Hernández, S.; Bertolín, J. R.; Cubel, C.; Castillo, J. R., Electrochemical affinity biosensors for detection of mycotoxins: A review. *Biosensors and Bioelectronics* **2013,** *49*, 146-158.
41. Jayasena, S. D., Aptamers: an emerging class of molecules that rival antibodies in diagnostics. *Clinical chemistry* **1999,** *45* (9), 1628-1650.
42. Ellington, A. D.; Szostak, J. W., In vitro selection of RNA molecules that bind specific ligands. *Nature* **1990,** *346* (6287), 818-822.
43. Tuerk, C.; Gold, L., Systematic evolution of ligands by exponential enrichment: RNA ligands to bacteriophage T4 DNA polymerase. *Science* **1990,** *249* (4968), 505-510.
44. Zhou, W.; Huang, P.-J. J.; Ding, J.; Liu, J., Aptamer-based biosensors for biomedical diagnostics. *Analyst* **2014,** *139* (11), 2627-2640.
45. Pohanka, M.; Skládal, P., Electrochemical biosensors—principles and applications. *Journal of applied biomedicine* **2008,** *6* (2).
46. Hu, S.; Liu, C. C., Amperometric sensor for fish freshness based on immobilized multi-enzyme modified electrode. *Electroanalysis* **1997,** *9* (16), 1229-1233.
47. Niu, J.; Lee, J. Y., Bulk-modified amperometric biosensors for hypoxanthine based on sol–gel technique. *Sensors and Actuators B: Chemical* **2000,** *62* (3), 190-198.
48. Okuma, H.; Watanabe, E., Flow system for fish freshness determination based on double multi-enzyme reactor electrodes. *Biosensors and Bioelectronics* **2002,** *17* (5), 367-372.
49. Eggins, B. R., *Chemical sensors and biosensors*. John Wiley & Sons: 2002; Vol. 2.
50. Mo, J.-W.; Smart, W., Lactate biosensors for continuous monitoring. *Frontiers in Bioscience-Landmark* **2004,** *9* (6), 3384-3391.
51. Wang, J.; Schultze, J., Analytical electrochemistry. *Angewandte Chemie-English Edition* **1996,** *35* (17), 1998-1998.
52. Zhan, X.; Tang, W.; Dou, W.; Zhao, G., Disposable immunosensor for Escherichia coli O157: H7 based on a multi-walled carbon nanotube-sodium alginate nanocomposite film modified screen-printed carbon electrode. *Analytical Letters* **2013,** *46* (17), 2690-2704.
53. Li, Y.; Cheng, P.; Gong, J.; Fang, L.; Deng, J.; Liang, W.; Zheng, J., Amperometric immunosensor for the detection of Escherichia coli O157: H7 in food specimens. *Analytical Biochemistry* **2012,** *421* (1), 227-233.

54. Cosby, D. E.; Cox, N. A.; Harrison, M. A.; Wilson, J. L.; Buhr, R. J.; Fedorka-Cray, P. J., Salmonella and antimicrobial resistance in broilers: A review. *Journal of Applied Poultry Research* **2015,** *24* (3), 408-426.
55. Fei, J.; Dou, W.; Zhao, G., A sandwich electrochemical immunoassay for Salmonella pullorum and Salmonella gallinarum based on a AuNPs/SiO_2/Fe_3O_4 adsorbing antibody and 4 channel screen printed carbon electrode electrodeposited gold nanoparticles. **2015**.
56. Conneely, G.; Aherne, M.; Lu, H.; Guilbault, G. G., Development of an immunosensor for the detection of testosterone in bovine urine. *Analytica chimica acta* **2007,** *583* (1), 153-160.
57. Arévalo, F. J.; Messina, G. A.; Molina, P. G.; Zón, M. A.; Raba, J.; Fernández, H., Determination of progesterone (P4) from bovine serum samples using a microfluidic immunosensor system. *Talanta* **2010,** *80* (5), 1986-1992.
58. Bahadır, E. B.; Sezgintürk, M. K., Applications of electrochemical immunosensors for early clinical diagnostics. *Talanta* **2015,** *132*, 162-174.
59. Felix, F. S.; Angnes, L., Electrochemical immunosensors–a powerful tool for analytical applications. *Biosensors and Bioelectronics* **2018,** *102*, 470-478.
60. Kaya, H. O.; Cetin, A. E.; Azimzadeh, M.; Topkaya, S. N., Pathogen detection with electrochemical biosensors: Advantages, challenges and future perspectives. *Journal of Electroanalytical Chemistry* **2021,** *882*, 114989.
61. Bahadır, E. B.; Sezgintürk, M. K., Lateral flow assays: Principles, designs and labels. *TrAC Trends in Analytical Chemistry* **2016,** *82*, 286-306.
62. Eltzov, E.; Guttel, S.; Low Yuen Kei, A.; Sinawang, P. D.; Ionescu, R. E.; Marks, R. S., Lateral flow immunoassays–from paper strip to smartphone technology. *Electroanalysis* **2015,** *27* (9), 2116-2130.
63. Nguyen, V.-T.; Song, S.; Park, S.; Joo, C., Recent advances in high-sensitivity detection methods for paper-based lateral-flow assay. *Biosensors and Bioelectronics* **2020,** *152*, 112015.
64. Sajid, M.; Kawde, A.-N.; Daud, M., Designs, formats and applications of lateral flow assay: A literature review. *Journal of Saudi Chemical Society* **2015,** *19* (6), 689-705.
65. Basiri, A.; Heidari, A.; Nadi, M. F.; Fallahy, M. T. P.; Nezamabadi, S. S.; Sedighi, M.; Saghazadeh, A.; Rezaei, N., Microfluidic devices for detection of RNA viruses. *Reviews in medical virology* **2021,** *31* (1), 1-11.
66. Yeo, L. Y.; Chang, H. C.; Chan, P. P.; Friend, J. R., Microfluidic devices for bioapplications. *Small* **2011,** *7* (1), 12-48.
67. Liu, S.; Gu, Y.; Le Roux, R. B.; Matthews, S. M.; Bratton, D.; Yunus, K.; Fisher, A. C.; Huck, W. T., The electrochemical detection of droplets in microfluidic devices. *Lab on a Chip* **2008,** *8* (11), 1937-1942.
68. Hiramoto, K.; Ino, K.; Nashimoto, Y.; Ito, K.; Shiku, H., Electric and electrochemical microfluidic devices for cell analysis. *Frontiers in chemistry* **2019,** *7*, 396.
69. Mahato, K.; Kumar, A.; Maurya, P. K.; Chandra, P., Shifting paradigm of cancer diagnoses in clinically relevant samples based on miniaturized electrochemical nanobiosensors and microfluidic devices. *Biosensors and Bioelectronics* **2018,** *100*, 411-428.
70. Fang, T. H.; Ramalingam, N.; Xian-Dui, D.; Ngin, T. S.; Xianting, Z.; Kuan, A. T. L.; Huat, E. Y. P.; Hai-Qing, G., Real-time PCR microfluidic devices with concurrent electrochemical detection. *Biosensors and Bioelectronics* **2009,** *24* (7), 2131-2136.
71. Pavlovic, E.; Lai, R. Y.; Wu, T. T.; Ferguson, B. S.; Sun, R.; Plaxco, K. W.; Soh, H., Microfluidic device architecture for electrochemical patterning and detection of multiple DNA sequences. *Langmuir* **2008,** *24* (3), 1102-1107.

72. Tang, D.; Yuan, R.; Chai, Y., Magnetic control of an electrochemical microfluidic device with an arrayed immunosensor for simultaneous multiple immunoassays. *Clinical Chemistry* **2007,** *53* (7), 1323-1329.
73. Yetisen, A. K.; Akram, M. S.; Lowe, C. R., based microfluidic point-of-care diagnostic devices. *Lab on a Chip* **2013,** *13* (12), 2210-2251.
74. Jang, I.; Carrão, D. B.; Menger, R. F.; Moraes de Oliveira, A. R.; Henry, C. S., Pump-free microfluidic rapid mixer combined with a paper-based channel. *ACS sensors* **2020,** *5* (7), 2230-2238.
75. Jang, I.; Kang, H.; Song, S.; Dandy, D. S.; Geiss, B. J.; Henry, C. S., Flow control in a laminate capillary-driven microfluidic device. *Analyst* **2021,** *146* (6), 1932-1939.
76. Carrell, C.; Link, J.; Jang, I.; Terry, J.; Scherman, M.; Call, Z.; Panraksa, Y.; Dandy, D. S.; Geiss, B. J.; Henry, C., Point-of-Need Disposable ELISA System for COVID-19 Serology Testing. **2020**.
77. Samper, I. C.; Sánchez-Cano, A.; Khamcharoen, W.; Jang, I.; Siangproh, W.; Baldrich, E.; Geiss, B. J.; Dandy, D. S.; Henry, C. S., Electrochemical Capillary-Flow Immunoassay for Detecting Anti-SARS-CoV-2 Nucleocapsid Protein Antibodies at the Point of Care. *ACS sensors* **2021,** *6* (11), 4067-4075.
78. Ouellet-Morin, I.; Danese, A.; Williams, B.; Arseneault, L., Validation of a high-sensitivity assay for C-reactive protein in human saliva. *Brain, Behavior, and Immunity* **2011,** *25* (4), 640-646.
79. Punyadeera, C.; Dimeski, G.; Kostner, K.; Beyerlein, P.; Cooper-White, J., One-step homogeneous C-reactive protein assay for saliva. *Journal of immunological methods* **2011,** *373* (1-2), 19-25.
80. Mohamed, R.; Campbell, J.-L.; Cooper-White, J.; Dimeski, G.; Punyadeera, C., The impact of saliva collection and processing methods on CRP, IgE, and Myoglobin immunoassays. *Clinical and translational medicine* **2012,** *1* (1), 1-8.
81. Labat, C.; Temmar, M.; Nagy, E.; Bean, K.; Brink, C.; Benetos, A.; Bäck, M., Inflammatory mediators in saliva associated with arterial stiffness and subclinical atherosclerosis. *Journal of hypertension* **2013,** *31* (11), 2251.

Chapter 2: Development of a Covid-19 immunosensor and assay adaptions for incorporating into automated electrochemical capillary-driven immunoassay device

Summary

This work presents the development of an electrochemical immunoassay for highly sensitive detection of SARS-CoV-2 N-protein in inactivated virus samples using inexpensive carbon paste electrodes. The assay was optimized and adapted for use in an automated electrochemical capillary-driven immunoassay device using screen-printed carbon electrodes. The system for the automated device took advantage of passive adsorption of capture antibodies to the carbon electrode to create a manufacturing-friendly procedure for electrode functionalization and achieved electrode stability for over 7 weeks. Finally, the assembled device accomplished quantitative detection of SARS-CoV-2 N-protein after a single sample addition step. The work presented here was done in collaboration with Isabelle Samper, Wisarut Khamcharoen, Kaylee Clark, Kate McMahon, and Trey Pittman. Unless otherwise noted, the data and figures were collected and processed by me. Some figures included in publications were omitted from this chapter and some unpublished optimization figures were added to this chapter in an effort to highlight my own contributions to the project. Ultimately, this work resulted in two publications, the first of which presents electrochemical detection of SARS-CoV-2 N-protein in nasopharyngeal samples and is published in *Analytical Chemistry.* The second publication focuses on an electrochemical capillary-driven immunoassay for detection of SARS-CoV-2 and has been accepted to *ACS Measurement Science Au.*

Introduction

The outbreak of COVID-19, caused by the infectious severe acute respiratory syndrome coronavirus-2 (SARS-CoV-2), shed light on the need for developments in effective point-of-care diagnostics.[1] Constant efforts to combat the spread through improved diagnostics are reflected in the increasing number of COVID-19 tests approved by FDA and the number of works published in literature.[2-4] Despite the options available, the recommended and most sensitive testing option is reverse transcriptase polymerase chain reaction (rt-PCR). Rt-PCR tests detect the viral RNA and remain the gold standard for testing as they have the lowest limits of detection (LOD) and highest specificity.[5] However, this assay takes several hours to complete, so depending on the site of sample collection, it can take several days for a patient to receive a result.[6] Enzyme-linked immunosorbent assays (ELISAs) have also been used to detect COVID-19 antigen or antibodies and are highly sensitive, but also lengthy and require laboratory instrumentation.[6, 7]

Lateral flow assays (LFAs) have been gaining attention as a means to decrease the time to result and allow for diagnosis at the point of care with no laboratory personnel required.[8] Generally, the addition of a sample induces capillary flow through the cellulose device, and reagents dried within the device are delivered sequentially to the test and control lines, producing a colorimetric signal of two lines for a positive sample and one line for a negative sample. However, these devices are rightfully criticized for their lack of sensitivity and poor LODs, especially compared to more sophisticated techniques like ELISA.[9, 10]

Fluidic devices are an emerging technology that show promise in accessing and improving point-of-care diagnostic options. They have been developed to perform several traditionally lab-based techniques like RT-PCR, reverse transcriptase loop-mediated isothermal amplification (RT-LAMP), nested PCR, nucleic acid hybridization, ELISA, and fluorescence based assays.[11] By

reducing the sample volumes needed, these devices provide a platform that can control reactions, separations, delivery of reagents, and detections with high sensitivity, faster readouts, and a lower cost compared to the traditional techniques.[12]

There have been many attempts to automate multi-step assays like ELISA using fluidic devices, but many still require multiple user steps.[13] A paper-based device for automated sequential multi-step sandwich ELISA was developed by Apilux *et al.* in 2013,[14] but paper devices are known to suffer from slow and non-uniform flow and have difficulties with particle and reagent transport.[15, 16] Electrochemical detection, as opposed to colorimetric, is attractive because it can be quick, cost effective, accurate, highly sensitive, and easily quantitative.[17] There are many existing reports of improving the sensitivity of LFAs by incorporating electrochemical transducers. Electrochemical lateral-flow immunoassays (eLFIAs) show promise in enabling detection of various analytes with improved specificity and selectivity and the opportunity for accessible quantitative read-outs, especially if paired with emerging smart-phone readout technology.[18 13-16, 19]

Our group previously published a disposable, fluidic ELISA system for COVID-19 serology testing. The device was made of inexpensive PET films and double-sided adhesives (DSA) and enabled the detection of COVID-19 antibodies with the sensitivity of an ELISA while maintaining the ease of use of an LFA.[20] To take advantage of the potential benefits of electrochemical detection, our group also developed a similar fluidic device with incorporated stencil-printed carbon electrodes for a quantitative read-out.[21] While the ability to monitor previous exposure to COVID-19 is important from an epidemiological standpoint, it is not useful as a diagnostic tool.

This work describes the development of an electrochemical immunoassay for detection of SARS-CoV-2 nucleocapsid protein (N-protein). The N-protein was selected as the analyte due to previous reports of its clinical relevance in Covid-19 diagnostics.[22, 23] After optimization on stencil-printed

carbon electrodes for highly sensitive detection of N-protein in inactivated virus samples, the assay was adapted and re-optimized on screen-printed carbon electrodes with the intent of incorporating the electrodes in a capillary-driven fluidic device. This creates a one-step point of care device for quantitative detection and diagnosis of Covid-19.

Materials and Methods

Reagents: Silver/silver chloride paste, sodium hydroxide (99.99%), sodium chloride (99.5%), ferrous sulfate heptahydrate (99.6%), Tris (2-carboxy-ethyl) phosphine hydrochloride (TCEP), sucrose, thimerosal, casein from bovine milk, 3,3',5,5'-Tetramethylbenzidine (TMB) Liquid Substrate System for ELISA, N-Hydroxysuccinimide (NHS) (98%), Tween 20, Superblock (PBS) blocking buffer, and *N*-(3-Dimethylaminopropyl)-*N*′-ethylcarbodiimide (EDC) (97%), were purchased from Sigma Aldrich (St. Louis, USA). Magnesium chloride, boric acid (99.5%), sodium tetraborate decahydrate, and Tween 80 were purchased from Thermo Fisher (Fair Lawn, NJ USA). EDTA disodium salt dihydrate was purchased from J.T.Baker (Stroudsburg, PA, USA). Trehalose (100%) was purchased from Calbiochem (USA) and bovine serum albumin (BSA) was purchased from Equitech-Bio (Kerrville, TX).

Buffers. Solutions were prepared using 18.2 MΩ · cm water purified using a Milli-Q system (Milli-poreSigma, USA). 10 mM phosphate buffer solution (PBS) with 140 mM sodium chloride and 2.7 mM potassium chloride, pH 7.4 was prepared using a tablet according to package instructions (Research Products International, USA). 10 mM phosphate buffer solution with Tween20 (PBST) was made by adding Tween20 to PBS to a final concentration of 0.05%. Hanks Balanced Salt Solution (HBSS) was prepared by combining 0.14 M sodium chloride, 5 mM potassium chloride, 1 mM calcium chloride, 0.4 mM magnesium sulfate, 0.5 mM magnesium

chloride, 0.3 mM sodium phosphate, 0.4 mM potassium phosphate, and 4 mM sodium carbonate to make a 1 L solution in Millipore water. HBSST buffer was made by adding Tween80 (Fischer Scientific, USA) and Igepal (MP Biomedicals, USA) to HBSS to make a final concentration of 0.1% and 0.1%, respectively. Viral transport media (VTM) was prepared according to CDC guidelines by adding fetal bovine serum, gentamicin sulfate, and amphotericin B to HBSS to a final concentration of 2%, 50 mg/mL and 250 µg/mL, respectively.[24] VTMT was made by adding Tween80 and Igepal to VTM so that the final concentration of each surfactant was equal to 0.1%. Antibody immobilization buffer for passive adsorption was prepared by adding 0.0005% Tween 20 to PBS. 1x stable peroxide buffer (SPB) was prepared by diluting commercial 10x stable peroxide buffer 1:10 and adding 0.1% Igepal and 0.1% Tween 80. 1 M borate buffer, pH 8.5, was prepared by dissolving boric acid in water and adding sodium hydroxide. The buffer was then diluted to 50 mM in water. Drying buffer for conjugate release pad preparation was prepared as previously reported.[25] First, a 1M solution of EDTA was prepared in PBS. Ferrous sulfate was added to a concentration of 0.01 M. Then 4% trehalose and 0.1% BSA was added, and the solution was stored at 4°C for up to 3 months.

Blocking solutions: Blocking solutions used for optimizations consisted of Superblock™ (PBS) blocking buffer (ThermoFisher), casein (Sigma Aldrich, USA) diluted in PBS to 1.0%, 0.6%, 0.3%, and 0.2%, a solution of 0.5%BSA and 0.2% casein diluted in PBS, and 1.0% and 0.3% aged casein diluted in 50 mM borate buffer. To make aged casein solutions, a bulk solution of 6% aged casein was prepared as previously reported.[26] Briefly, 6 g of casein was dissolved in 80 mL of 50 mM sodium hydroxide overnight. Then 0.26 g boric acid and 0.45 g sodium tetraborate were added and the solution was pH adjusted to 8.5. The solution was diluted to 100 mL with Millipore distilled water and heated at 37°C for 7 days. The aged casein was aliquoted and stored at –20°C.

Electrode fabrication:

Stencil printed carbon electrodes (Figure 1(A)), used for initial assay development, blocker optimization, and calibration curve, were fabricated using a PET film stencil, cut with a CO_2 laser to form a working, counter, and reference electrode system. A carbon composite mixture of 3:5 TC303 graphite (Asbury Carbons, USA) and carbon ink (Ercon, USA) was mixed until homogenous then stencil printed on a PET film and dried at 60°C for 30 minutes. Ag/AgCl paste (Sigma Aldrich, USA) was then painted over the reference electrode and dried at 60°C for 30 minutes. Double-sided adhesive wells (3M, USA) were laser cut (8 mm in diameter) and adhered to expose a circle over the working, counter, and reference electrodes.

Screen-printed carbon electrodes (Figure 1(B)), used for optimizations for fluidic device and in fluidic experiments, were created by screen printing on 3M 2500 PET film using carbon ink and a 305-count mesh screen. After printing, the ink was dried for 30 min at 60°C. Dielectric ink wells were then screen-printed around the working electrode and UV cured until dry. Reference electrode was painted over with a thin layer of Ag|AgCl paste (Sigma-Aldrich Saint Louis, MO) and dried for 30 min at 60°C. For fluidic experiments, the electrode coversheets (PET sheets on which electrodes were screen printed) were then cut using a CO_2 laser cutter according to the device layout and serve as top layer of the device. For static experiments, a double-sided adhesive well (3M, USA) was attached over the working, counter, and reference electrodes to mimic the fluidic channel.

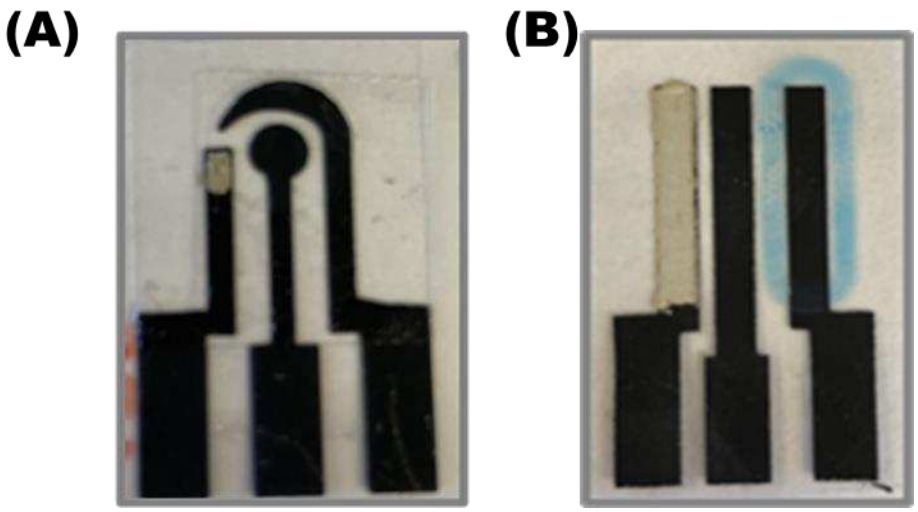

Figure 2.1: Pictures of stencil-printed carbon electrode (A) and screen-printed carbon electrode with di-electric ink well (B).

Antibodies used for initial assay evaluation and optimization of blocking conditions:

House-made anti-N antibodies. Rabbit polyclonal anti-bodies targeting SARS-CoV-2 N protein were prepared as previously described.[27, 28] Briefly, rabbits were immunized by Pacific Immunology with truncated SARS-CoV-2 nucleocapsid antigen (AA133-416) produced and purified in E. coli. Hyperimmune serum was passed over a SARS-CoV-2 nucleocapsid column and binding antibodies eluted and collected. Eluted antibody preparations were dialyzed against PBS with 0.1% sodium azide and stored at –20°C until use. These were prepared by James Terry and Loran Anderson.

House-made anti-N-HRP. Anti-N antibodies prepared as described above were first purified using a NucAway spin column (Invitrogen by Thermo Fisher Scientific, USA) according to package instructions. Once purified, antibodies were conjugated to horseradish peroxidase (HRP)

using a Lightening-Link® HRP-Conjugation kit (Abcam, UK) according to kit instructions. Stock antibody was diluted to 0.5 µg/mL in HBSST. This solution was prepared by Kate McMahon.

Electrode modification and assay measurements

Stencil-printed electrodes were functionalized with a 20 µL aliquot of 10 µg/mL capture antibody using EDC/NHS coupling. First, 20µL of 5 mM EDC/NHS in water was dropped over the working electrode (WE) and incubated for 45 minutes. The solution was then removed, and a 20 µL aliquot of capture antibody, diluted in PBS, was dropped and incubated for 60 minutes. The capture antibody solution was removed, and the electrode was washed with PBST followed by PSB. The electrode was then blocked with a 50 µL aliquot of the specified blocking solution for 60 minutes and washed again with PBST and PBS. Virus samples, diluted in VTM, were dropped and incubated for 40 minutes, then removed and rinsed with PBST and PBS. HRP-labeled antibody, 0.5 µg/mL diluted in PBS+0.5%BSA, was then incubated for 25 minutes, removed and washed with PBST and PBS. PBS was dropped on the electrode to stabilize and prevent drying until electrochemical measurements could be taken.

Screen-printed electrodes were functionalized through passive adsorption of a 10 µL aliquot of 10 µg/mL MM08 capture antibody (Sino Biological, USA) allowed to dry on the WE at 37°C. The WE was then blocked with 5 µL of 0.3% aged casein solution. DSA wells were added after functionalization for static assay measurements. For static assay experiments, wells made with 3M 467 double sided adhesive (DSA) mimicking the size of the fluidic channel were placed over the working, counter, and reference electrodes to confine the solutions. To complete the assay, 20 µL of inactivated virus, diluted in SPB, was dropped in the well and incubated for 30 min. After washing with PBST followed by PBS, 20 µL of 1 µg/mL labeled antibody (MM05-H) solution in

SPB was dropped into the well and incubated for 25 min. The electrodes were washed a final time, and 20 µL of PBS was dropped until measurements could be taken.

Static assay measurements on both stencil and screen-printed electrodes were obtained by removing PBS just before the measurement. 50 µl of TMB was then added to the electrode surface, confined by the adhesive well, and incubated for 2 min. Immediately following the TMB incubation, a 2-min amperometry measurement was started using a potentiostat (PalmSens4). A 0.0 V potential was applied to the working electrode (vs the Ag|AgCl reference electrode), while the current was recorded.

Fluidic device preparation and assembly. Un-modified glass fiber with PVA binder (Millipore) was cut to make 3x5 mm^2 conjugate release pads. The pads were pre-treated by soaking in a solution containing PBS, 0.01% thimerosal, 0.5% Tween 20, and 3% w/v sucrose for 45 minutes. Pads were then removed and dried at 37°C overnight until completely dry. Device layers 1-4 were cut and assembled using a CO_2 laser prior to experiments. HRP antibody conjugate release pads were prepared by drying 10 µL of 20 µg/mL de-salted MM05-HRP antibody (diluted in drying buffer) onto pre-treated glass fiber in 5 µL aliquots with 5 min drying time at 37°C after each aliquot. Then 5 µL of yellow dye, diluted 1:80 in water, was added to the pad and pads were completely dried at 37°C for at least 1 hour. TMB pads were prepared by drying 15 µL of commercial TMB solution, in 5 µL aliquots with 5 minutes drying at 37°C after each aliquot, onto pre-treated glass fiber pads. Then 5 µL of blue dye, diluted 1:80 in water, was added and pads were completely dried at 37°C for at least 1 hour. Once dry, conjugate release pads were place in the channels of the fluidic device, and the cover-layer, containing the modified electrode were place on top and the device was manually pressed to seal.

Fluidic assay measurements. The modified electrode coversheets and reagent pads were prepared as described above. 95 µL of sample was added to the inlet of the device to initiate flow and sequential delivery of reagents and the device was connected to PalmSens4. Once the blue dye visibly reached the detection channel, a 0.0 V potential was applied and current was measured until the peak was complete.

Electrochemical Data Processing. For the data collected using the static detection method, the current from the amperograms was averaged over 10 s centered at 60 s for triplicate measurements unless otherwise noted. Change in current (ΔI) was calculated from the difference in averages from the blank to target signal. For fluidic experiments, the highest point of the current peak from the amperogram was averaged for each device for three devices.

Results and Discussion:

Electrode modification and preliminary results. In an ELISA, a capture element specific to the analyte of interest is immobilized on a platform and binds to the target analyte in a positive sample.[29] **Figure 2.2(A)** shows a schematic of the sandwich ELISA that occurs at the stencil-printed electrode surface, enabling the detection of SARS-CoV-2 recombinant N-protein. The capture antibody (red) is immobilized on the graphitic electrode surface via EDC/NHS coupling. Following immobilization, the surface is blocked to reduce the opportunity for non-specific adsorption. When the sample is introduced, the target protein (yellow diamond) binds to the capture antibody. Next, a horseradish peroxidase (HRP)-labeled antibody is introduced and binds to any virus protein that was captured. Upon the introduction of TMB substrate, the HRP catalyzes the oxidation of TMB. The oxTMB is then reduced as the potential is held at 0.0V, generating an electrochemical signal. **Figure 2.2(B)** demonstrates the expected result for a sample containing SARS-CoV-2 N-protein. Measurements in this study were recorded by first allowing the substrate

to incubate for 120 seconds, then holding a constant potential of 0.0 V and recording current for 120 seconds. **Figure 2.2(C)** presents preliminary data collected before any optimizations were made. This data shows a concentration dependent signal as seen in the large difference from the blank for the 100 ng/mL sample (green) compared to the 10 ng/mL sample (purple). The NL63 protein (orange) was used as a proof of concept to show the specificity of the assay. Control points were recorded showing the assay in the absence of capture antibody (blue), and without HRP-labeled antibody (red). The no HRP control yielded a current lower than that of the blank, indicating some non-specific adsorption of the HRP-antibody to the electrode surface or the auto-oxidation of TMB possibly from light. Interestingly, the "no capture" antibody control resulted in a current between that of the 10 ng/mL and 100 ng/mL concentrations of target protein. This indicates a significant amount of non-specific adsorption of the target analyte to the electrode surface and need for further optimization.

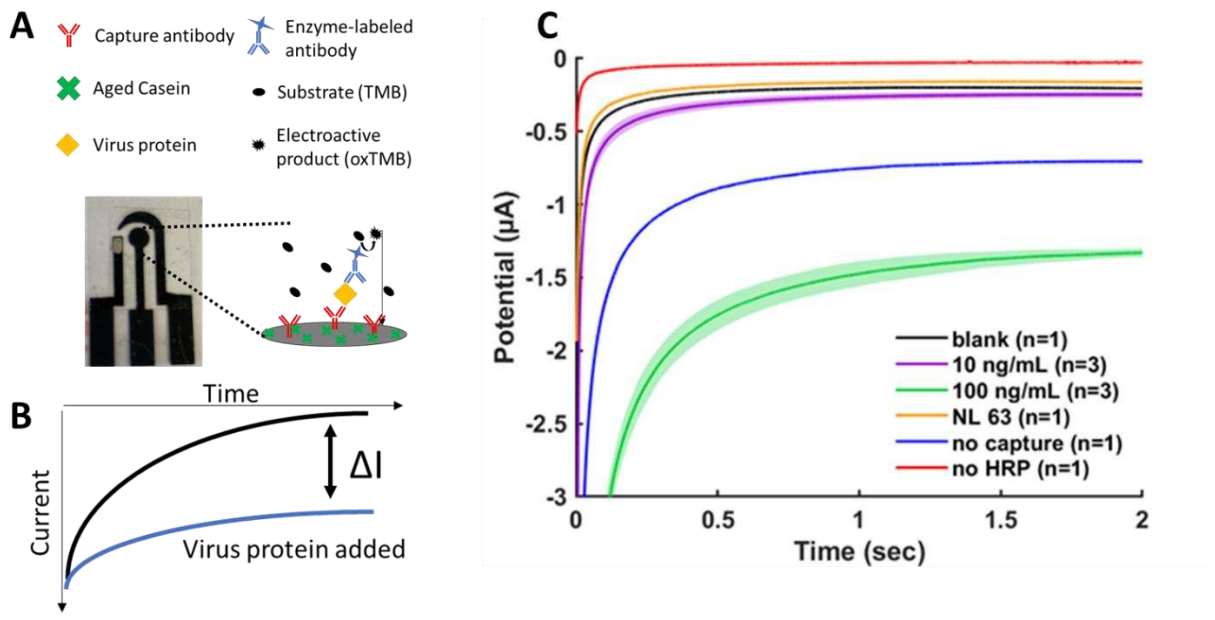

Figure 2.2: (A) Picture of a fabricated stencil-printed carbon electrode with accompanying schematic of immunoassay and detection mechanism showing electrode modified with capture antibody, blocked to prevent non-specific adsorption, target virus protein, labeled secondary

antibody, and electrochemically active substrate. **(B)** Representative amperogram depicting the expected change in signal as the concentration for target protein in the sample increases. **(C)** Preliminary amperometry data showing a concentration-dependent signal for recombinant N-protein at 0 (n=1), 10 (n=3), and 100 ng/mL (n=3) (black, purple, and green respectively), no interference for competing protein NL63 (orange) (n=1), no signal without enzyme-labeled secondary antibody (red) (n=1), and some signal from non-specific adsorption of SARS-CoV-2 N-protein (blue) (n=1).

Optimization of Electrode Blocking Step. Many optimization experiments were performed to improve upon preliminary data. Due to the urgency of the project, the work was divided among the team. This dissertation only includes optimization experiments that were completed by me. One of the large contributions to this was the evaluation of different solutions for the assay blocking step, intended to prevent non-specific adsorption of proteins and other bio-fouling agents to the electrode surface.[30] A series of four experiments was performed, each evaluating three different blocking solutions. The change in current from the blank for each are plotted in **Figure 2.3** with **(A)** presenting the ΔI for a 10 ng/mL N-protein sample and **(B)** presenting ΔI for a 100 ng/mL sample. Each set of three solutions was evaluated to determine the "best" considering signal and error before moving on, which is why some conditions were repeated in further experiments. Finally, it was determined that the 0.3% aged casein would be used for future experiments based on the high signal for both concentrations tested. Aged casein has previously been used to prevent non-specific signal in a nitrocellulose LFA for Covid-19 antigen detection.[26]

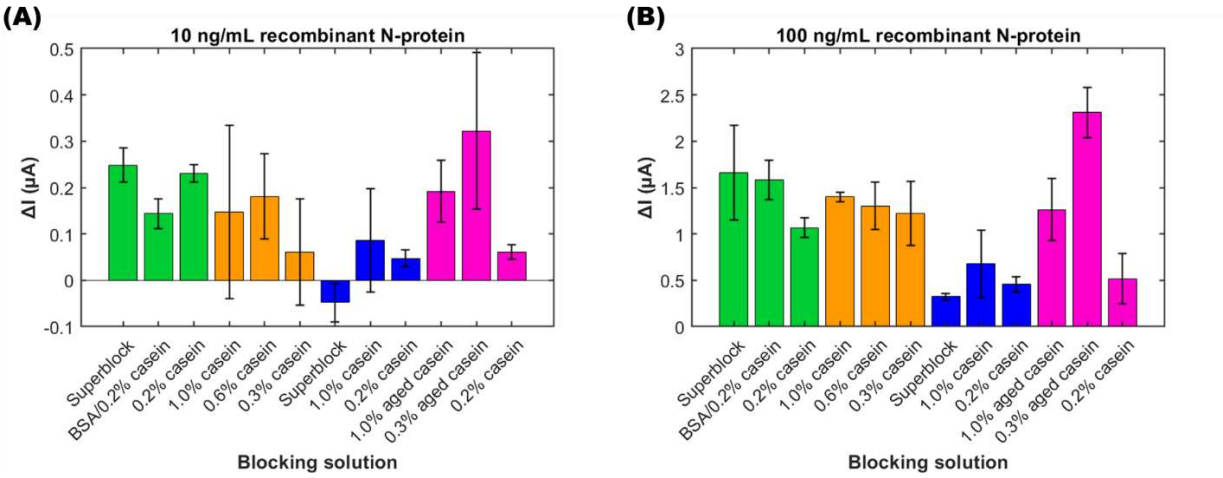

Figure 2.3: Bar graphs representing ΔI for 10 ng/mL **(A)** and 100 ng/mL **(B)** recombinant N-protein samples with varying solutions used for the blocking step. Colors on the graph represent experiments that were performed on the same day. Each set of 3 conditions was evaluated for the best results before moving forward. Height of bars indicates the change in current for triplicate measures of blank and target samples.

Optimized assay performance. After adjusting the assay according to optimizations, samples containing inactivated SARS-CoV-2 virus ranging from 0 – 110,000 PFU/mL were tested on the system. For each point, a 20 µL aliquot of inactivated virus, diluted in VTM, was added to a well over a functionalized electrode surface and incubated for 40 minutes, then removed and the electrodes was washed with PBST and PBS. Next, a 20 µL aliquot of 0.5 µg/mL HRP-labeled antibody in (buffer) was added, incubated for 25 minutes, removed, and washed. PBS was dropped on the electrode to stabilize until measurements could be taken. For measurements, the buffer was removed and a 50 µL aliquot of TMB was incubated for 2 minutes, then a 0.0 V potential was applied for 2 minutes and current was measured. **Figure 2.4A** shows the average signal (line) and standard deviation (shading) from 3 electrodes for each concentration point tested. There was a difference from the blank, even for the lowest concentration of 220 PFU/mL, and the signal increased with each virus concentration up to 22,000 PFU/mL. It is important to note that the signal

for 110,000 PFU/mL is lower than the signal for 22,000 PFU/mL. This can be attributed to the hook effect, which is common in immunoassays.[30] **Figure 2.4B** shows the calibration curve developed calculating ΔI averaged over a 10-second interval centered at t=100 seconds. The change in current increases for each concentration point except 110,000 PFU/mL and the curve was follows a 4-parameter logistic (4PL) model, which is typical for immunoassays.[31, 32] The calculated limit of detection for the assay resulting from 3 times the standard deviation of the blank is an impressive 45 PFU/mL. For comparison, most commercially available rapid antigen tests for Covid-19 report an LOD ranging from 80 – 500 PFU/mL.[33, 34] It is important to note that the lowest concentration tested for this assay was 220 PFU/mL whereas the LOD reported for commercially available tests is a concentration that was tested. However, the 220 PFU/mL tested in this study still falls within the reported range.

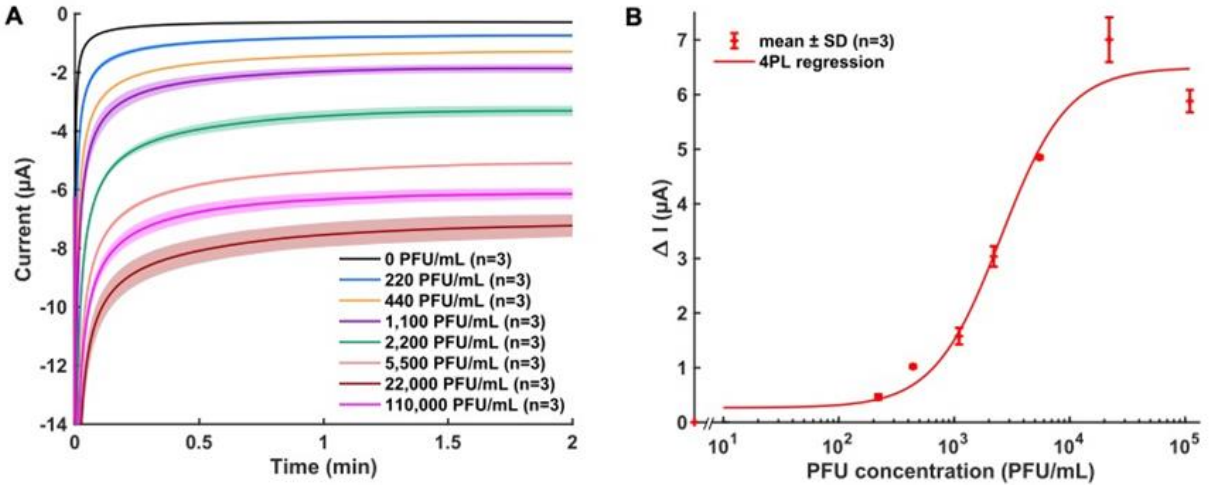

Figure 2.4: (A) Amperometric detection of 20 µL aliquots of varying concentrations of inactivated SARS-CoV-2 virus. Lines and shaded areas represent averages and standard deviations, respectively, of triplicates. (B) Corresponding calibration curve reporting ΔI for triplicate measurements calculated over an averaged 10 s interval centered at t=100 s. Data was fit with a 4-parameter logistic (4PL) regression. LOD calculated from the blank signal plus 3 times the standard deviation of the blank is 45 PFU/mL. Acknowledgement: This data was collected and plotted by Isabelle Samper and Catherine McMahon.

Adapting for automated fluidic assay system. While the limit of detection for the developed assay was impressive, the assay still required trained personnel and took several hours to complete. To develop a more user-friendly system, a capillary driven fluidic device was created to automate sequential reagent delivery and washing steps, but the stencil-printed electrodes used for the previous studies were not compatible with the fluidic system. The thickness of the electrodes caused leaking through the DSA and inhibited flow. For these reasons, thinner screen-printed carbon electrodes were used for subsequent studies.

Figure 2.5(A) shows an exploded view of the 5-layer fluidic device. The polyethylene terephthalate (PET) films (gray) and double-sided adhesive (red) are patterned with a CO_2 laser and sandwiched together, resulting in hollow channels of varying depths, a single sample inlet, and a paper waste pad that serves as a passive pump. Two conjugate release pads, stored within the device, contain reagents necessary to complete the sandwich ELISA. **Figure 2.5(B)** illustrates sequential delivery of the reagents (represented with dye) dried in the pads to the electrode surface with washes between reagent delivery that occurs via capillary action upon the addition of a 100 µL sample. **Figure 2.5(C)** is a schematic of the sandwich ELISA that occurs at the electrode surface during the assay. Capture antibody is immobilized on the screen-printed working electrode and the surface is blocked using aged casein prior to assembly of the device. The addition of sample to the device induces flow and delivers the protein present in the sample to the electrode **(Figure 2.4 (B) (i))**, allowing the virus particles to be captured at the electrode surface. As flow continues, the HRP-labeled antibody is delivered to the electrode **(Figure 2.5 (B) (ii))** and binds to the virus present. Finally, the substrate is delivered across the electrode **(Figure 2.4 (B) (iii))** and generates an electrochemical current in the presence of HRP. This results in a peak in the amperogram as the TMB flows across the electrode surface.

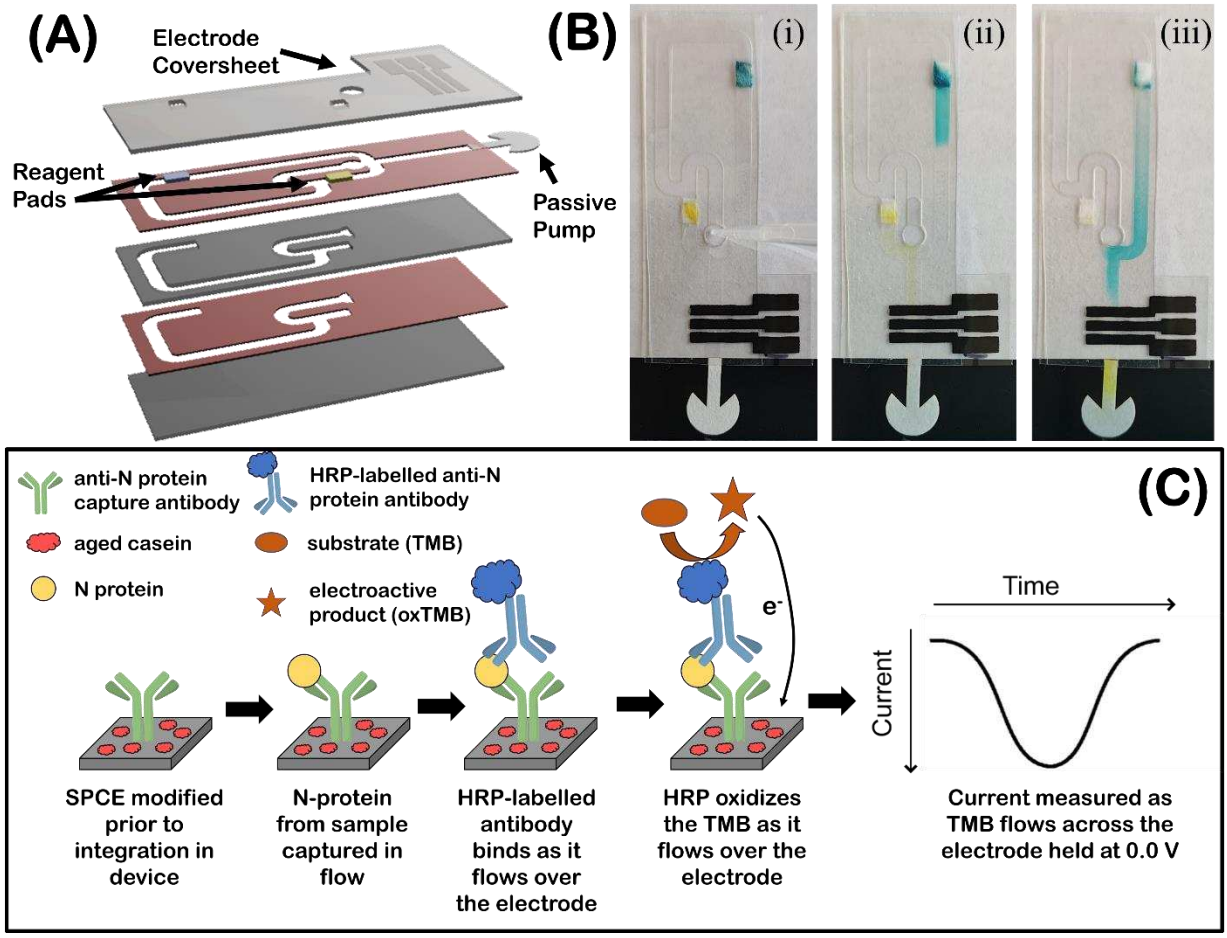

Figure 2.5: (A) Exploded view of eCaDI showing alternating PET (gray) and adhesive (red) layers. The second layer from the top shows the two reagent pads (blue = TMB, yellow= HRP ab) and the passive pump on the far right. **(B)** Flow of eCaDI (i) Addition of sample and sequential delivery of (ii) HRP-Antibodies (with yellow dye) and (iii) TMB (with blue dye) to the SPCE. **(C)** Electrochemical immunoassay and detection mechanism, showing modified electrode, target capture, secondary antibody binding, turnover of substrate, and electrochemical detection. Acknowledgement: This figure was made by Kaylee Clark.

Optimization of electrode and assay components. Electrodes were screen printed using a 305-size mesh screen with either a mixture of TC303 graphite with Ercon ink (used for previous experiments) and a commercially available carbon ink. Optimization studies were carried out using different combinations of capture antibody (house-made rabbit antibodies and commercial MM08

antibodies) and analytes (house-made recombinant N-protein and inactivated virus) on each of the carbon types. Due to the number of electrodes needed for this study, two separate experiments were performed. **Figure 2.6** presents the change in current recorded for each condition. **(A)** represents the data collected for the TC303/Ercon ink electrodes while **(B)** represents the data collected on commercial CI2057 electrodes. The first two bars in each plot (shaded in green) represent Experiment 1 and the last two bars (orange) represent experiment 2. For the TC303 electrodes, the rabbit antibody with recombinant N-protein had the largest ΔI, but also higher error than the other points. The MM08 with recombinant N-protein and MM08 with inactivated virus seemed to perform comparably. Surprisingly, the commercial CI2057 carbon ink yielded a higher ΔI for the MM08/virus and MM08/NP combinations compared to any signal from the TC303 electrodes. Based on this data, the optimized parameters for further experiments were the CI2057 electrodes, modified with MM08 capture antibodies, and inactivated virus samples as the analyte.

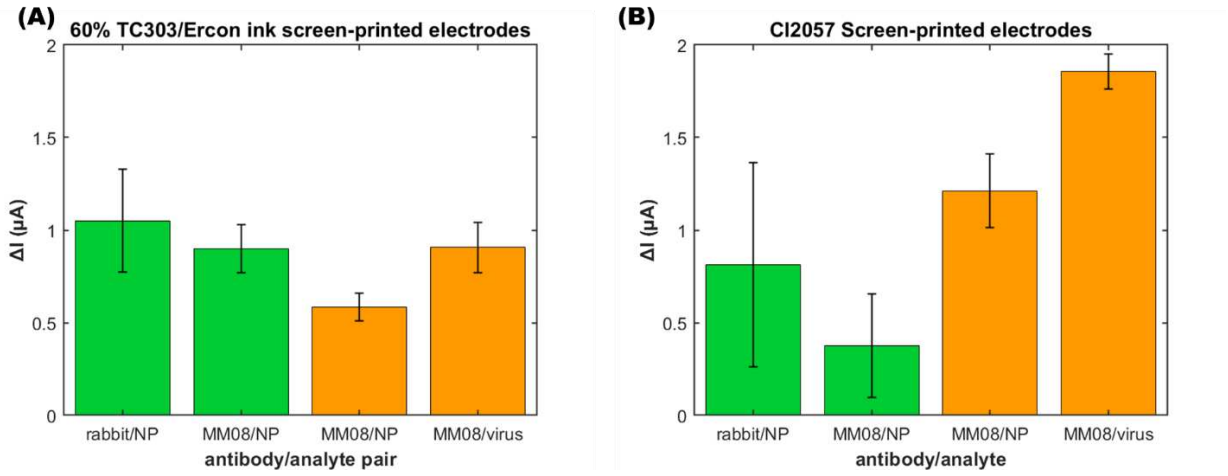

Figure 2.6: Bar graphs plotting the change in current (ΔI) for various combinations of capture antibody and corresponding analyte. Bar heights were calculated from the difference in target from blank current of triplicate amperometric measurement currents averaged over a 10 s interval centered at t = 60 s. Error bars represent standard deviation of the triplicate measurements. Bars shaded with green were collected in one experiment while bars shaded in blue were collected in another. **(A)** Electrode modification and static assay was carried out using screen printed electrodes

made with 60% TC303 graphite in Ercon ink. (**B)** Electrodes for these data were screen printed using un-modified commercial CI2057 ink.

Optimization of electrode modification. The EDC/NHS coupling of the antibody to the electrode surface required long incubations and manual washing steps that would be difficult to scale up for manufacturing and distribution of this device. A previous report indicated that passively adsorbed antibodies on bare carbon electrodes preformed similar or better in terms of LOD and sensitivity than immobilization techniques like covalently binding to gold nanoparticles (AuNP), chitosan, and reduced graphene oxide (rGO).[35] Further, passive adsorption would eliminate the need for incubations and washing steps. For this study, passive antibody adsorption through drop-casting and drying the capture antibody, followed by drying aged casein blocker was explored. This method required two simple pipetting steps to prepare the electrodes for assay measurements. **Figure 2.7(A)** evaluates the change in signal achieved for a 20 µL sample of 690 PFU/mL inactivated virus using a static assay. For this experiment, capture antibody was de-salted and diluted to 5, 10, and 20 µg/mL (first quantified using Solo-VP) in PBS + 0.0005% Tween 20. The Tween 20 was added to help with the spreading of the solution. 10 µL of solution was dropped in the di-electric well over the working electrode and manually spread to cover the entire well. Left in ambient conditions, the electrodes were visibly dry in about 35 minutes. Then a 5 µL aliquot of 0.3% aged casein in borate buffer was dropped in the WE well and was visibly dry in about 10 minutes. The 10 µg/mL capture antibody concentration resulted in the highest change in signal, and the 5 µg/mL concentration was just slightly lower and had similar error bars. The highest concentration, 20 µg/mL resulted in the lowest signal and highest error. Due to the complexity and time required for the quantification of the capture antibody, 10 µg/mL, un-quantified and assumed no dilution from de-salting was the parameter selected for the capture antibody. It was assumed

that the actual concentration would fall somewhere between 5 and 10 µg/mL, both of which resulted in good signal and low error.

Conditions for antibody drying were explored to increase signal. For the first experiment (**Figure 2.7(B)** (blue) 10 µL of a 10 µg/mL capture antibody solution (described previously) was dropped and spread over the WE. The electrodes were then placed in a sealed petri dish, desiccator, or left in ambient conditions. After 2 hours, the electrodes in the petri dish were not visibly dry, so the seal was removed, and they were allowed to finish drying under ambient conditions. The electrodes in the desiccator dried in about 25 minutes and the electrodes under ambient conditions dried in about 20 minutes. The set dried in the petri dish resulted in the highest ΔI and lowest error. In a second experiment (green) the petri-dish drying method was compared to drying in an incubator at 37°C. The set dried at 37°C resulted in an even higher change in signal with comparable error. Thus, for future experiments, electrodes were dried under these conditions.

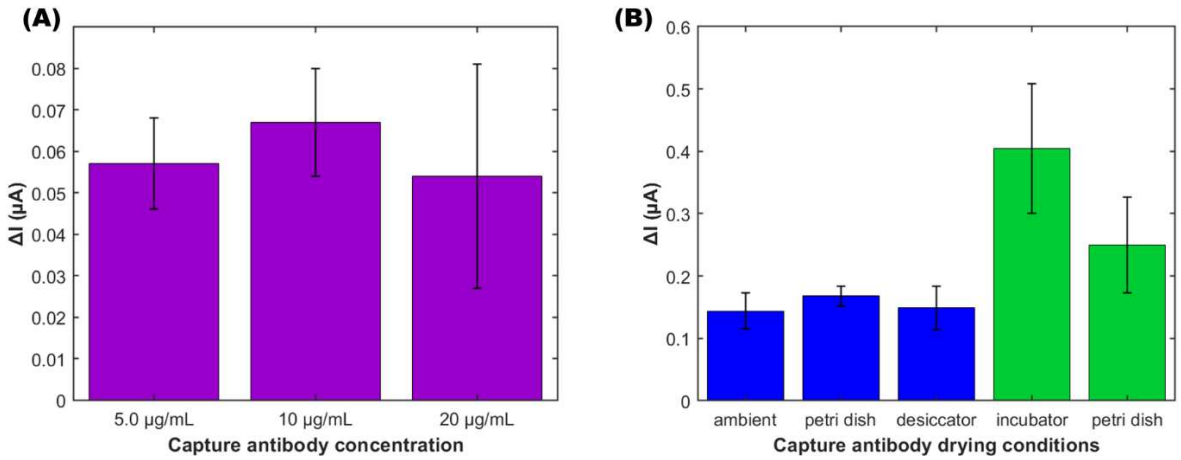

Figure 2.7: Bar graphs plotting the change in current (ΔI) vs. parameters optimized for electrode functionalization. Bar heights were calculated from the difference in target from blank current of triplicate amperometric measurement currents averaged over a 10 s interval centered at t = 60 s. Error bars represent standard deviation of the triplicate measurements. **(A)** Compares ΔI for 690 PFU/mL virus solution, determined via static assay procedures on electrodes modified with varying capture antibody concentrations. **(B)** Compares ΔI for a 2750 PFU/mL virus solution with 10 µg/mL capture antibody dried under varying conditions. Note, the first three points (blue) were

collected on a different day and with different solutions than the last two (green). Acknowledgement: Trey Pittman helped with these experiments.

Optimization of assay components. Moving toward an automated fluidic device, Hanks buffer, used previously, was impractical due to the complexity of the buffer and the need for H_2O_2 to turnover the dried substrate. Further, the optimal buffer would need to be compatible with both the inactivated virus binding and binding of the HRP antibody as the device design only allows for addition of a single sample. Commercially available stable peroxide was explored to ease the transition to large-scale manufacturing of the diagnostic device. A surfactant, Igepal, was added at 0.1% to help break apart the virus particles, releasing the N-protein for binding. 300 mM NaCl was also added to the SPB to increase the ionic strength of the solution. **Figure 2.8(A)** compares ΔI for static assay measurements of a 20 µL sample of 2750 PFU/mL inactivated virus using Hanks buffer (pH 6.5), commercial stable peroxide buffer diluted to 1x (unaltered pH 5.5), and 1X commercial stable peroxide buffer (pH adjusted to 6.5) for dilution of both the inactivated virus and HRP antibody (diluted to 0.5 µg/mL). The Hanks buffer (used for previous studies) resulted in the highest ΔI, but also the largest standard deviation. The SPB pH did not seem to have a large effect on the signal, therefore, SPB at pH = 5.5 was chosen for the remaining experiments due to the ease of use.

The concentration of HRP antibody needed to achieve the best signal in the static assay was evaluated by testing the static assay while varying the concentration of HRP antibody. **Figure 2.8(B)** shows the ΔI calculated under each of these conditions. In the first experiment (green), it was determined that the change in signal increased with the concentration of HRP antibody. However, the standard deviation also increased greatly from 1 µg/mL to 3 µg/mL. Note, the concentrations reported here are assumed based on the dilution factor and do not account for any

dilution of the antibody that could have occurred in the de-salting process. It is likely that the concentration was lower than what is reported. A second experiment was performed evaluating HRP-antibody concentrations of 0.5, 1, and 2 µg/mL (assumed concentrations) (orange) and a quantified aliquot of 1 µg/mL (pink). Contrary to previous results, the highest change in signal was seen in the 1 µg/mL assumed concentration but this point also had a larger standard deviation compared to 0.5 and 2 1 µg/mL. Interestingly, the aliquot calculated using a variable path length technique had both a large ΔI and the lowest error bars seen in these experiments. This is likely due to a slight variance in surfactant concentration as the de-salted antibody was first diluted 1:10 in PBS to achieve the appropriate volume for quantification, and later diluted further in SPB for use in the assay.

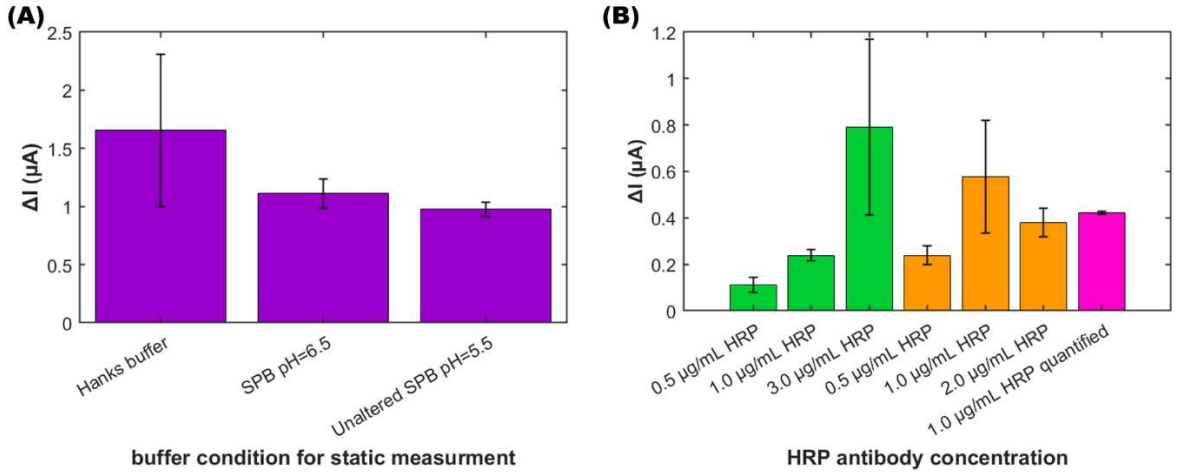

Figure 2.8: Bar graphs plotting the change in current (ΔI) vs. parameters optimized for assay procedures working toward fluidic device. Bar heights were calculated from the difference in 2750 PFU/mL target from blank current of triplicate amperometric measurement currents averaged over a 10 s interval centered at t = 60 s. Error bars represent standard deviation of the triplicate measurements. Electrodes were functionalized using optimized parameters. **(A)** Change in current for varied buffers used for dilution of inactivated virus and HRP-labeled antibody. **(B)** Change in current from varied concentrations of HRP antibody. Unless otherwise noted, HRP antibody concentration was calculated based on dilution factor, not accounting for dilution from de-salting.

The first 3 points (green) were collected in a different experiment form the last four (orange and pink).

Evaluation of manufacturing-friendly modification. To compare the newly optimized modification procedure to the previous static incubations on stencil printed electrodes shown in **Figure 2.4**, the new functionalization technique was used to measure varying concentrations of inactivated SARS-CoV-2 virus following similar assay incubation steps. Here, the untreated screen-printed carbon electrodes were functionalized with capture antibody by drop-casting 10 µL of a 10 µg/mL antibody solution on the working electrode and spreading to fill the di-electric ink well. The solution was dried at 37 C until visibly dry (about 40 minutes). Aged casein was then dropped in the WE well and allowed to dry in ambient conditions (about 15 minutes) to block un-modified active sites on the electrode surface and reduce the opportunity for non-specific adsorption. The new modification technique reduced the time for functionalization from 1.75 h to under 1 h and eliminated the need for manual washing steps. For this study, subsequent assay steps were carried out in a similar manner to that of the static assay for comparison purposes. **Figure 2.9(A)** shows the chronamperometric response to varying concentrations of inactivated SARS-CoV-2 virus. There was a clear difference from the blank for each concentration tested ranging from 340 PFU/mL to 11,000 PFU/mL with the signal increasing for each of the higher concentrations. The figure shows a representative curve for each concentration point which were performed in triplicates. **Figure 2.9(B)** shows the corresponding calibration curve plotting the average blank subtracted current vs the concentration of virus in the sample. The data was fit with a dose response logistic fit which is expected for immunoassays.[36, 37] The LOD for this assay, calculated using the theoretical blank plus 3 times the SD of the blank, was 68 PFU/mL. While this LOD is higher than reported using the previous assay functionalization technique, the

simplified modification lends itself to large-scale manufacturing, and the calculated LOD still falls within the range reported for commercially available rapid antigen tests.

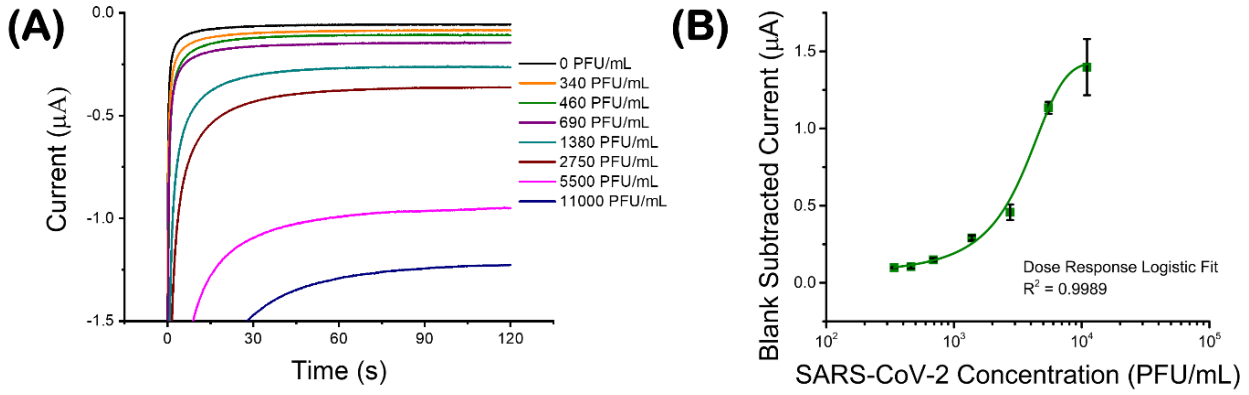

Figure 2.9: (A) Representative amperograms for varying concentrations of inactivated SARS-CoV-2 virus in SPB taken on modified electrodes using the static electrochemical detection method. **(B)** Corresponding calibration curve plotted on a log scale showing blank subtracted current for triplicate measurements. Symbols and error bars represent average and standard deviation over a 10 s interval centered on 60 s (n=3). Data is fit with a dose response logistic fit. Acknowledgement: This data was plotted by Kaylee Clark.

Evaluation of potential for storage. An important characteristic necessary for a point-of-care diagnostic device is the ability to store under reasonable conditions for long periods of time. To this end, a study was done to evaluate the performance of the electrodes over time when stored under varying conditions. Similar to Figure 6, the performance of the electrodes was determined using a static assay procedure for measurements. **Figure 2.10(A)** shows the blank-subtracted current for a 1380 PFU/mL sample when stored at room temperature and 4-5 C, with and without desiccant, over 24 days. Each data point was determined from triplicates of each the blank and target. As shown in the figure, the modified electrodes were most stable when stored with desiccant, at room temperature. Other works have also reported that desiccant is necessary to reduce the opportunity for protein degradation in humid environments.[38-40] However, it is

surprising that the electrodes stored better at ambient conditions because this contradicts previous reports on antibody-based sensors.[38, 41] While the exact mechanism to explain this is unknown, we speculate that either the higher humidity levels in the refrigerator, despite the desiccant, contributed to protein degradation, or the cold temperatures negatively impact the performance of the screen-printed electrodes.

The optimal storage condition, room temperature with desiccant, was then evaluated over almost 8 weeks. **Figure 2.10(B)** shows the blank subtracted signal for a 1380 PFU/mL sample at different time points. Each point on the plot represents the average blank subtracted signal, determined by n=5 for target and n=3 for blanks. The data shows that the signal remains relatively constant between 0.09 and 0.13 μA over the almost eight weeks. The standard deviation did increase substantially after 4 weeks but remained easily differentiable from the blank. This is an improvement over previous reports.[41] In addition to effects from long-term storage, variation in the data can be attributed to inconsistencies stemming from making the virus and HRP-antibody solutions fresh for each point, as well as inconsistencies in electrode fabrication and modification. Regardless, the stability of the electrodes over this time period is a promising step toward point-of-care sensors that require the ability for long-term storage.

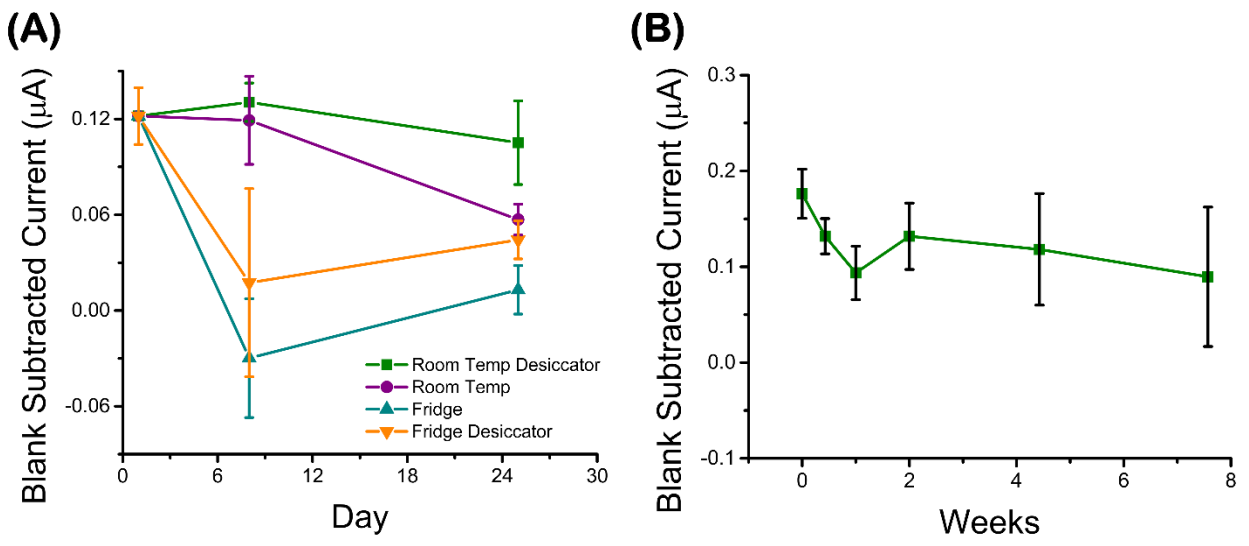

Figure 2.10: (A) Plot showing stability of functionalized electrodes at ambient temperature and 4-5 C, with and without desiccant. Each point represents the average change in current from chronpamperometric data averaged over a 10 s interval centered at 60 s from n=3 target and n=3 blank. **(B)** Plot showing stability of functionalized electrodes stored in a desiccator at ambient temperature. Each point represents the average change in current from chronoamerometric data averaged over a 10 s interval centered at 60 s from n=3 blank and n=5 target._Acknowledgement: This data was plotted by Kaylee Clark.

Fully automated electrochemical capillary-driven immunoassay. Optimized parameters from this work were used in the fully automated electrochemical capillary-driven immunoassay for detection of SARS-CoV-2 inactivated virus samples. For this study, 100 µL of sample was added to the inlet of the device shown in **Figure 2.5.** The addition of the sample induced capillary flow and delivered the virus, followed by the HRP-labeled antibody and TMB substrate across the electrode surface. Amperometry data was collected from the time the TMB began flowing across the electrode (seen with blue dye added to the pad) until the peak reached a steady state current. Representative peaks for a blank sample and four concentration points are shown in **Figure 2.11(A). Figure 2.11(B)** plots the average peak height for 3 devices run with the given concentration. While this was not enough data for a curve to fit, there was a clear increase in the peak height with each concentration point, indicating a concentration-dependent signal.

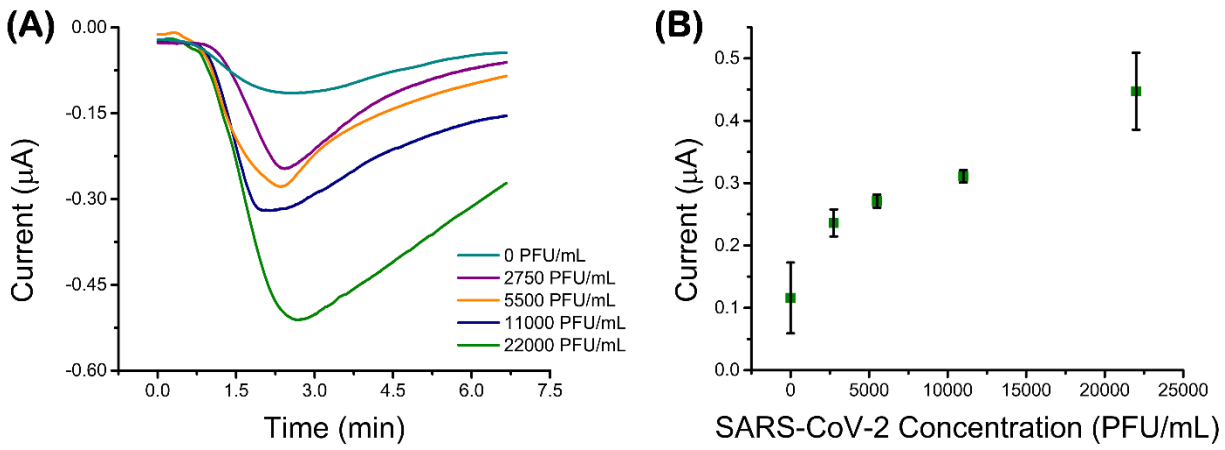

Figure 2.11: (A) Representative amperograms from full eCaDI device for varying concentration of SARS-CoV-2 in SPB (n=3). Potential was held at 0.0 V for the duration of the runs. Data was time-aligned with TMB delivery to the electrode. **(B)** Corresponding plot of various concentrations of inactivated SARS-CoV-2 virus in SPB. Symbols and error bars represent average and standard deviation of peak current from amperograms (n=3 for each blank and concentration). Acknowledgement: This data was collected and plotted by Kaylee Clark

Conclusions and future directions:

This work demonstrates the steps necessary to develop an immunoassay with electrochemical detection, and modifications and optimizations that need to be made for automation. This is an important process to enable the development of accessible, point-of-care diagnostic options to help combat crises, like the Covid-19 pandemic, and to improve health outcomes overall by enabling widespread diagnostic options. The work presented here was able to successfully detect various concentrations of SARS-CoV-2 N-protein using the fully automated device. However, more work is needed to achieve necessary requirements for large-scale manufacturing distribution. First, the assay still has a great deal of variability in fluidic dynamics from one device to another as seen in highly variable reagent delivery times. Many devices assembled did not flow correctly, and data could not be obtained. Further, the time required for read-out (about 30 minutes), made it difficult

to perform larger-scale experiments and more data points would be helpful for further analysis of the device.

Going forward, focus on adapting the fluidic device for more consistent reagent delivery and faster assay run times will help enable further studies of this system and move towards larger-scale production. After device optimizations, the system can be tuned for diagnosis of other viral proteins by switching the capture and label antibodies. The development of this platform technology will help provide point-of-care diagnostic options that have not been previously available.

References

1. Ji, T.; Liu, Z.; Wang, G.; Guo, X.; Lai, C.; Chen, H.; Huang, S.; Xia, S.; Chen, B.; Jia, H., Detection of COVID-19: A review of the current literature and future perspectives. *Biosensors and Bioelectronics* **2020,** *166*, 112455.

2. Giri, B.; Pandey, S.; Shrestha, R.; Pokharel, K.; Ligler, F. S.; Neupane, B. B., Review of analytical performance of COVID-19 detection methods. *Analytical and bioanalytical chemistry* **2021,** *413* (1), 35-48.

3. Rai, P.; Kumar, B. K.; Deekshit, V. K.; Karunasagar, I.; Karunasagar, I., Detection technologies and recent developments in the diagnosis of COVID-19 infection. *Applied microbiology and biotechnology* **2021,** *105* (2), 441-455.

4. Song, Q.; Sun, X.; Dai, Z.; Gao, Y.; Gong, X.; Zhou, B.; Wu, J.; Wen, W., Point-of-care testing detection methods for COVID-19. *Lab on a Chip* **2021,** *21* (9), 1634-1660.

5. van Kasteren, P. B.; van Der Veer, B.; van den Brink, S.; Wijsman, L.; de Jonge, J.; van den Brandt, A.; Molenkamp, R.; Reusken, C. B.; Meijer, A., Comparison of seven commercial RT-PCR diagnostic kits for COVID-19. *Journal of Clinical Virology* **2020,** *128*, 104412.

6. Weissleder, R.; Lee, H.; Ko, J.; Pittet, M. J., COVID-19 diagnostics in context. *Science translational medicine* **2020,** *12* (546), eabc1931.

7. Carter, L. J.; Garner, L. V.; Smoot, J. W.; Li, Y.; Zhou, Q.; Saveson, C. J.; Sasso, J. M.; Gregg, A. C.; Soares, D. J.; Beskid, T. R., Assay techniques and test development for COVID-19 diagnosis. ACS Publications: 2020.

8. Chau, C. H.; Strope, J. D.; Figg, W. D., COVID-19 clinical diagnostics and testing technology. *Pharmacotherapy: The Journal of Human Pharmacology and Drug Therapy* **2020,** *40* (8), 857-868.

9. Mahmoudinobar, F.; Britton, D.; Montclare, J. K., Protein-based lateral flow assays for COVID-19 detection. *Protein Engineering, Design and Selection* **2021,** *34*.

10. Ong, D. S.; De Man, S.; Lindeboom, F. A.; Koeleman, J. G., Comparison of diagnostic accuracies of rapid serological tests and ELISA to molecular diagnostics in patients with suspected coronavirus disease 2019 presenting to the hospital. *Clinical Microbiology and Infection* **2020,** *26* (8), 1094. e7-1094. e10.

11. Basiri, A.; Heidari, A.; Nadi, M. F.; Fallahy, M. T. P.; Nezamabadi, S. S.; Sedighi, M.; Saghazadeh, A.; Rezaei, N., Microfluidic devices for detection of RNA viruses. *Reviews in medical virology* **2021,** *31* (1), 1-11.

12. Yeo, L. Y.; Chang, H. C.; Chan, P. P.; Friend, J. R., Microfluidic devices for bioapplications. *small* **2011,** *7* (1), 12-48.

13. Jeong, S.-G.; Kim, J.; Jin, S. H.; Park, K.-S.; Lee, C.-S., Flow control in paper-based microfluidic device for automatic multistep assays: A focused minireview. *Korean Journal of Chemical Engineering* **2016,** *33* (10), 2761-2770.

14. Apilux, A.; Ukita, Y.; Chikae, M.; Chailapakul, O.; Takamura, Y., Development of automated paper-based devices for sequential multistep sandwich enzyme-linked immunosorbent assays using inkjet printing. *Lab on a Chip* **2013,** *13* (1), 126-135.

15. Gong, M. M.; Sinton, D., Turning the page: advancing paper-based microfluidics for broad diagnostic application. *Chemical reviews* **2017,** *117* (12), 8447-8480.

16. Nguyen, M. P.; Meredith, N. A.; Kelly, S. P.; Henry, C. S., Design considerations for reducing sample loss in microfluidic paper-based analytical devices. *Analytica chimica acta* **2018,** *1017*, 20-25.
17. Kaya, H. O.; Cetin, A. E.; Azimzadeh, M.; Topkaya, S. N., Pathogen detection with electrochemical biosensors: Advantages, challenges and future perspectives. *Journal of Electroanalytical Chemistry* **2021,** *882*, 114989.
18. Cheng, J.; Yang, G.; Guo, J.; Liu, S.; Guo, J., Integrated electrochemical lateral flow immunoassays (eLFIAs): recent advances. *Analyst* **2022,** *147* (4), 554-570.
19. Mak, W. C.; Beni, V.; Turner, A. P., Lateral-flow technology: From visual to instrumental. *TrAC Trends in Analytical Chemistry* **2016,** *79*, 297-305.
20. Carrell, C.; Link, J.; Jang, I.; Terry, J.; Scherman, M.; Call, Z.; Panraksa, Y.; Dandy, D. S.; Geiss, B. J.; Henry, C., Point-of-Need Disposable ELISA System for COVID-19 Serology Testing. **2020**.
21. Samper, I. C.; Sánchez-Cano, A.; Khamcharoen, W.; Jang, I.; Siangproh, W.; Baldrich, E.; Geiss, B. J.; Dandy, D. S.; Henry, C. S., Electrochemical Capillary-Flow Immunoassay for Detecting Anti-SARS-CoV-2 Nucleocapsid Protein Antibodies at the Point of Care. *ACS sensors* **2021,** *6* (11), 4067-4075.
22. Li, T.; Wang, L.; Wang, H.; Li, X.; Zhang, S.; Xu, Y.; Wei, W., Serum SARS-COV-2 nucleocapsid protein: a sensitivity and specificity early diagnostic marker for SARS-COV-2 infection. *Frontiers in cellular and infection microbiology* **2020,** *10*, 470.
23. Shan, D.; Johnson, J. M.; Fernandes, S. C.; Suib, H.; Hwang, S.; Wuelfing, D.; Mendes, M.; Holdridge, M.; Burke, E. M.; Beauregard, K., N-protein presents early in blood, dried blood and saliva during asymptomatic and symptomatic SARS-CoV-2 infection. *Nature communications* **2021,** *12* (1), 1-8.
24. CDC Posts New Standard Operating Procedure for Creating Viral Transport Media. https://www.cdc.gov/csels/dls/locs/2020/new_sop_for_creating_vtm.html (accessed July 18, 2022).
25. Ramachandran, S.; Fu, E.; Lutz, B.; Yager, P., Long-term dry storage of an enzyme-based reagent system for ELISA in point-of-care devices. *Analyst* **2014,** *139* (6), 1456-1462.
26. Grant, B. D.; Anderson, C. E.; Williford, J. R.; Alonzo, L. F.; Glukhova, V. A.; Boyle, D. S.; Weigl, B. H.; Nichols, K. P., SARS-CoV-2 coronavirus nucleocapsid antigen-detecting half-strip lateral flow assay toward the development of point of care tests using commercially available reagents. *Analytical chemistry* **2020,** *92* (16), 11305-11309.
27. Fagre, A.; Lewis, J.; Eckley, M.; Zhan, S.; Rocha, S. M.; Sexton, N. R.; Burke, B.; Geiss, B.; Peersen, O.; Bass, T., SARS-CoV-2 infection, neuropathogenesis and transmission among deer mice: Implications for spillback to New World rodents. *PLoS Pathogens* **2021,** *17* (5), e1009585.
28. Terry, J. S.; Anderson, L. B.; Scherman, M. S.; McAlister, C. E.; Perera, R.; Schountz, T.; Geiss, B. J., Development of a SARS-CoV-2 nucleocapsid specific monoclonal antibody. *Virology* **2021,** *558*, 28-37.
29. Clark, M. F.; Lister, R. M.; Bar-Joseph, M., ELISA techniques. In *Methods in enzymology*, Elsevier: 1986; Vol. 118, pp 742-766.
30. Tate, J.; Ward, G., Interferences in immunoassay. *The clinical biochemist reviews* **2004,** *25* (2), 105.

31. O'Connell, M.; Belanger, B.; Haaland, P., Calibration and assay development using the four-parameter logistic model. *Chemometrics and Intelligent Laboratory Systems* **1993,** *20* (2), 97-114.
32. Heineman, W. R.; Halsall, H. B., Strategies for electrochemical immunoassay. *Analytical chemistry* **1985,** *57* (12), 1321A-1331A.
33. Cubas-Atienzar, A. I.; Kontogianni, K.; Edwards, T.; Wooding, D.; Buist, K.; Thompson, C. R.; Williams, C. T.; Patterson, E. I.; Hughes, G. L.; Baldwin, L., Limit of detection in different matrices of 19 commercially available rapid antigen tests for the detection of SARS-CoV-2. *Scientific reports* **2021,** *11* (1), 1-8.
34. Corman, V. M.; Haage, V. C.; Bleicker, T.; Schmidt, M. L.; Mühlemann, B.; Zuchowski, M.; Jo, W. K.; Tscheak, P.; Möncke-Buchner, E.; Müller, M. A., Comparison of seven commercial SARS-CoV-2 rapid point-of-care antigen tests: a single-centre laboratory evaluation study. *The Lancet Microbe* **2021,** *2* (7), e311-e319.
35. Sharafeldin, M.; McCaffrey, K.; Rusling, J. F., Influence of antibody immobilization strategy on carbon electrode immunoarrays. *Analyst* **2019,** *144* (17), 5108-5116.
36. Dudley, R.; Edwards, P.; Ekins, R.; Finney, D.; McKenzie, I.; Raab, G.; Rodbard, D.; Rodgers, R., Guidelines for immunoassay data processing. *Clinical chemistry* **1985,** *31* (8), 1264-1271.
37. Cox, K. L.; Devanarayan, V.; Kriauciunas, A.; Manetta, J.; Montrose, C.; Sittampalam, S., Immunoassay methods. *Assay Guidance Manual [Internet]* **2019**.
38. Kaduskar, O.; Bhatt, V.; Prosperi, C.; Hayford, K.; Hasan, A. Z.; Deshpande, G. R.; Tilekar, B.; Vivian Thangaraj, J. W.; Kumar, M. S.; Gupta, N., Optimization and stability testing of four commercially available dried blood spot devices for estimating measles and rubella IgG antibodies. *Msphere* **2021,** *6* (4), e00490-21.
39. Flounders, A.; Brandon, D.; Bates, A., Patterning of immobilized antibody layers via photolithography and oxygen plasma exposure. *Biosensors and Bioelectronics* **1997,** *12* (6), 447-456.
40. Li, X.; Liu, X., A microfluidic paper-based origami nanobiosensor for label-free, ultrasensitive immunoassays. *Advanced healthcare materials* **2016,** *5* (11), 1326-1335.
41. Li, F.; You, M.; Li, S.; Hu, J.; Liu, C.; Gong, Y.; Yang, H.; Xu, F., based point-of-care immunoassays: Recent advances and emerging trends. *Biotechnology advances* **2020,** *39*, 107442.

Chapter 3: Electrochemical aptamer-based assay for measurement of CRP in automated fluidic device

Summary:

This work describes an electrochemical aptamer-based assay for the detection and quantification of C-reactive protein, a biomarker of inflammation commonly measured in clinical settings. The assay follows a similar procedure to a typical immunoassay but takes advantage of the benefits of aptamers as opposed to antibodies as biological recognition elements. A fluidic device is also described to automate the assay steps with sequential delivery and washing. The device design allows for the incorporation of commercially available DropSens electrodes, that can be externally functionalized for protein detection. Finally, this work compares the aptamer-based assay on carbon electrodes to the performance on gold electrodes. Ongoing and future experiments aim to optimize the device to reduce non-specific signal and test with varying concentrations of CRP and with saliva samples before publication.

Introduction:

C-reactive protein (CRP) is an acute-phase protein (APP) whose levels in human serum change drastically in response to inflammatory conditions.[1] It is commonly measured as a marker of systemic inflammation[2] and also to monitor the progression of diseases and treatments based on changes from an established baseline.[3] Some studies show that CRP levels can also serve as an independent risk factor for cardiovascular disease.[2, 4] Given the widespread clinical applications, a significant amount of research has been done to enable monitoring of CRP levels.[5-10] Enzyme-linked immunosorbent assays (ELISAs) are a highly sensitive detection method commonly used to measure proteins like CRP. However, these assays are time consuming and require trained

personnel, expensive equipment, and laboratory settings. To increase the accessibility of these measurements, there is an increasing focus on developing point of care (POC) testing devices. Lateral flow assays (LFAs) have been developed to enable single-step detection at the point of care. These typically function by capillary action through a nitrocellulose strip to deliver sample and reagents dried within the device across a detection zone. They usually include a test and control line, resulting in the appearance of a single line for a negative sample and a double line for a positive sample. Unfortunately, these devices usually underperform with regards to sensitivity and limits of detection (LODs) relative to traditional assays.[11, 12] Many efforts have been made to improve the performance of LFAs by incorporating electrochemical transducers.[13] In 1999, Lee *et al.* developed a liposome immunosensor for theophylline detection by incorporating a thick film electrode underneath a traditional nitrocellulose strip.[14] Rismetov *et al.* took advantage of developments in nanomaterials to develop a sensor for H_2O_2 using electro-deposited boron-doped diamond (BDD) and platinum nanoparticles. In 2018, Dempsey *et al.* developed an immunosensor using an antibody-functionalized electrode with a lateral flow membrane for detection of Troponin T and explored the effects of blocking agents.[15] Other notable examples of these devices include detection a wide variety of analytes ranging from hormones like testosterone,[16] to large proteins like troponin[17] and albumin,[18] viruses like H1N1,[19] and others.[13]

In clinical settings, CRP assays usually require serum extracted from a whole blood sample. Moving toward a non-invasive sample, many researchers have looked to develop a CRP assay for detection in saliva samples.[20-22] While there are some conflicting reports,[23, 24] some studies report a strong correlation between salivary CRP and serum CRP levels, with salivary levels being significantly lower.[25-28] Clinical levels of CRP in healthy individuals range from 0.14 to 31.1 mg/L in human plasma,[23] while salivary CRP levels have been reported with values of 0.05 to 64.3

ng/mL[23] and as low as 35 to 217 pg/mL.[27] Considering this, sensitivity is of great importance in measurements of CRP in saliva. Current challenges in using saliva samples for POC diagnostics are the influence of the oral environment on CRP levels, the collection of a standardized sample, and the extraction of biomarkers reproducibly from the complex sample matrix.[29] Recent developments have included a photothermal biosensor for detection of CRP in saliva[30] and CRP detection in human saliva using nanoplasmonic color imaging.[31] While achieving great sensitivity, these techniques are not compatible with POC testing.

A recent publication from Petruzzi *et al.* reported concentration-dependent detection of CRP using an electrochemical sensor with an LFA platform. This allowed for single step addition of sample and quantitative CRP detection. However, although this work achieved an LOD of 3 ng/mL in buffer, it increased to 25 ng/mL in saliva, so better sensitivity is needed to measure the entire dynamic range of CRP in saliva.[32] Using this platform, the sample and enzyme-labeled antibody flow through a porous nitrocellulose strip, providing ample opportunity for loss of analyte to the nitrocellulose pores and compromising sensitivity.

Our group recently demonstrated flow control and mixing in a laminate capillary-driven microfluidic device.[33] An external cellulose waste pad inserted in the outlet of the device wicks fluid through the channels, greatly reducing the opportunity for sample loss within the device. Later, we reported a capillary-driven fluidic system using alternating layers of CO_2 patterned polyethylene terephthalate (PET) films and double-sided adhesive (DSA) to create hollow channels that accomplished sequential delivery of reagents across a test line. This was used to automate the steps of an ELISA.[34] Further work presented an electrochemical capillary-driven immunoassay for detection of SARS-CoV-2 N-protein. Here, functionalized screen-printed electrodes were incorporated in the laminate fluidic device for electrochemical detection of the

sandwich immunoassay.[35] This was an important step in the development of POC diagnostics, but the assay was limited by the time to results, inconsistencies in flow, variability in devices, and the need for improved sensitivity.

While immunoassays have historically reported highly specific and sensitive detection of biological analytes, aptamers provide some interesting advantages for use as biological recognition elements in place of antibodies. Aptamers are nucleic acids that fold into 3D structures that bind with high affinity and specificity to a given analyte.[36] They are chemically synthesized, which reduces the batch-to-batch variation that is likely with antibodies and makes them easily functionalized for various applications.[37, 38] Some reports indicate the opportunity to improve the sensitivity of traditional immunoassays through the use of aptamers due to their strong binding affinities and stability compared to antibodies.[36, 39] There are many previous reports of aptasensors for CRP detection.[40-43] While these studies provided important steps in optimizing conditions for aptamer binding,[40] achieved highly sensitive detection with an LOD of 5 fg/mL,[41] simplified detection through the use of electrochemical sensors,[42] and simplified sensor functionalization with the use of a DNA aptamer,[43] they still required trained personnel and laboratory settings and equipment, making them not useful for point of care measurements. Chen *et al.* recently published a rapid fluorescent aptasensor for CRP detection, but this device still required 40 minutes to achieve a result.[44]

This work aims to develop a point of care device for measurements of CRP in human saliva in 10 minutes. Using an automated capillary-driven device, reagents are sequentially delivered across an aptamer-functionalized screen-printed gold electrode surface. Signal is generated by an enzyme-substrate reaction that is proportional to the concentration of CRP in the sample, yielding a quantitative readout.

Materials and Methods:

Reagents: Silver/silver chloride paste, sodium hydroxide (99.99%), sodium chloride (99.5%), ferrous sulfate heptahydrate (99.6%), Tris (2-carboxy-ethyl) phosphine hydrochloride (TCEP), sucrose, thimerosal, casein from bovine milk, 6-Mercapto-1-hexanol (MCH) (97%), 3,3',5,5'-Tetramethylbenzidine (TMB) Liquid Substrate System for ELISA, N-Hydroxysuccinimide (NHS) (98%), Tween 20, Superblock (PBS) blocking buffer, and *N*-(3-Dimethylaminopropyl)-*N*′-ethylcarbodiimide (EDC) (97%), were purchased from Sigma Aldrich (St. Louis, USA). Magnesium chloride, boric acid (99.5%), sodium tetraborate decahydrate, and Tween 80 were purchased from Thermo Fisher (Fair Lawn, NJ USA). Tris-HCl (99.4) and EDTA disodium salt dihydrate were purchased from J.T.Baker (Stroudsburg, PA, USA). PBS tablets containing 0.010 M Phosphate buffer pH = 7.4, 0.0027 M KCl, and 0.14 M NaCl were purchased from Medicago (Sweden). Ethanolamine (ACS Reagent grade) was purchased from MP Biomedical (Solon, OH, USA). Trehalose (100%) was purchased from Calbiochem (USA) and bovine serum albumin (BSA) was purchased from Equitech-Bio (Kerrville, TX). CRP Protein (95%) and CRP antibody were purchased from Fitzgerald Industries Inc. (Acton, MA).

Solutions: Solutions were prepared using 18.2 MΩ · cm water purified using a Milli-Q system (Milli-poreSigma, USA). Phosphate buffered saline (10mM) was prepared by dissolving commercial tablets according to instructions. PBST was prepared by adding 0.05% Tween 20 in PBS. CRP binding buffer was prepared containing 100 mM Tris-HCl, 100 mM NaCl, and 10 mM $MgCl_2$. TrisT wash buffer was prepared by adding 0.05% Tween 20 to CRP binding buffer. HRP antibody buffer was prepared by adding 0.5% BSA and 0.1% Tween 80 to CRP binding buffer. Drying buffer solution was prepared by adding 0.01 M EDTA, 0.01 M $FeSO_4$, 4% trehalose, and 0.1% BSA to PBS. This was stored refrigerated (4-5 C) for no more than 3 months. Anti-CRP-

HRP was prepared using a Lightning Link conjugation kit (Abcam, USA) according to instructions.

Aptamers: Aptamers used for experiments include a thiol-terminated CRP DNA aptamer used for experiments with gold electrodes and an amine-terminated aptamer used for experiments with carbon electrodes. Both were purchased from Integrated DNA Technologies (Coralville, IA). The aptamer sequence matched that of previous reports.[42, 43, 45, 46] The nucleic acid sequence is as follows:

Thiolated: 5'- /5ThioMC6-D/GCC TGT AAG GTG GTC GGT GTG GCG AGT GTG TTA GGA GAG ATT GC -3'

Amine-terminated: 5'- /5AmMC6/GCC TGT AAG GTG GTC GGT GTG GCG AGT GTG TTA GGA GAG ATT GC -3'

Before immobilization on electrodes, thiol-terminated aptamer was treated with 200x TCEP for 2 hours to reduce di-sulfide bonds following protocol from the manufaturer.[47] Both aptamers were treated by heat shocking before use in immobilization. The aptamer solution was heated at 95-100°C for 5 minutes, then cooled at 0°C for 10 minutes, and allowed to come to room temperature for 15 minutes.

Electrode preparation and functionalization: Commercial screen-printed gold electrodes (DRP220 AT, Metrohm USA) were cleaned using cyclic voltammetry from -0.2 to 1.15 V at 100 mV/s for 10 scans in a 150 µL solution of 0.5 M H_2SO_4. After cycling, electrodes were purged with nitrogen for about 10 minutes. 20 µL of heat-shocked 1 nM aptamer solution was drop-casted on to the working electrode. Electrodes were placed in a sealed humidity chamber and kept at 4-5°C overnight (about 16 hours). Aptamer solution was then removed, and electrode was rinsed 3

times with 150 µL PBS. 100 µL of 1 mM MCH blocking solution was dropped on electrode and incubated for 60 minutes, then removed and washed with PBST and PBS. The electrodes were allowed to dry, then were used in fluidic devices or for static measurements where indicated.

For experiments using stencil-printed carbon electrodes, a mixture of 60% TC303 graphite (Asbury Carbon, Warren County, NJ) was mixed with E3178 Carbon ink (Ercon, Wareham, MA) and printed using PET film stencils. Electrodes were dried at 60°C for 30 minutes, then reference electrodes were painted with Ag|AgCl paste and dried at 60°C for another 30 minutes. 3M DSA wells were pressed over electrodes to contain solutions. To functionalized electrodes, 50 µL of a solution containing 2.5 mM EDC and 2.5mM NHS in water was dropped over the working electrode and incubated for 45 minutes. This solution was removed and a solution containing 50 µL of 1 nM amine-terminated CRP aptamer in PBS was dropped over the working electrode, incubated for 60 minutes, then removed and electrodes were washed with PBST and PBS. The electrode was the blocked with a solution containing 0.5% ethanolamine in PBS for 60 minutes, then washed with PBST and PBS.

For static measurements on both gold and carbon electrodes, 100 µL CRP in binding buffer was incubated for 30 minutes, then removed and electrodes were washed with TrisT and CRP binding buffer. Then 100 µL of 1 µg/mL anti-CRP-HRP in HRP antibody buffer was incubated for 30 minutes, removed, and electrodes were washed again with TrisT and CRP binding buffer. 100 µL of CRP binding buffer was added until measurements could be taken. Amperometry data was obtained by removing the CRP binding buffer and dropping 100 µL of commercial TMB, incubating for 120 seconds, then holing a 0.0 V potential and measuring current for 120 seconds.

Preparation of reagent pads for fluidic device: Un-modified glass fiber with PVA binder (Millipore) was cut to make 3x5 mm^2 conjugate release pads. The pads were pre-treated by soaking

in a solution containing PBS, 0.01% thimerosal, 0.5% Tween 20, and 3% w/v sucrose for 45 minutes. Pads were them removed and dried at 37°C overnight until completely dry.

HRP antibody reagent pads were prepared by adding two 5 µL aliquots of 20 µg/mL anti-CRP-HRP diluted in drying buffer (or drying buffer + 0.5% BSA where indicated) to a pre-treated pad with 5 minutes of drying time at 37°C after each aliquot. Then 5 µL of generic yellow food dye (diluted 1:80 in water) was added to the pad and dried for at least 1 hour at 37°C. TMB reagent pads were preparred by adding three 5 µL aliquots of commercial TMB to each pad with 5 minutes of drying time at 37°C after each aliquot. 5 µL of generic blue food dye (diluted 1:80 in water) was added and pads were dried for at least 1 hour at 37°C before device assembly.

Device assembly and fluidic measurements: Alternating layers of polyethylene terephthalate (PET) sheets (9984) and 467 double-sided adhesive (DSA) (3M, USA) were cut using a CO_2 laser and sandwiched together prior to experiments. Dried reagent pads were placed in the fluidic channels and the cover layer was attached. The modified electrode was placed in the template over the outlet channel and manually pressed to seal. A 25 mm Whatman 4 chromatography paper waste pad was inserted to the end of the outlet channel just before measurement. For measurements, 100 µL of sample was added to the inlet of the device to initiate flow. Amperometric measurements were taken from 5 minutes after sample addition to 10 minutes after sample addition by applying a 0.0 V potential and measuring current.

Data processing: Static amperometry data was evaluated by averaging a 10 s interval centered at 60 s for triplicate measurements.

Results and Discussion:

Aptasensor schematic for CRP detection: An aptasensor is like an immunosensor in its construction but uses an aptamer as the biological recognition element as opposed to an antibody. An aptamer is a nucleic acid sequence that folds into a 3D structure that can bind with high affinity and specificity to non-nucleic acid analytes.[48, 49] In this work, an aptasensor was created to measure CRP using commercial screen-printed gold electrodes (SPGE). **Figure 3.1** illustrates the steps of the assay that take place to achieve detection of CRP. First, thiolated aptamer is immobilized on the working electrode overnight, then the surface is blocked with mercaptohexanol (MCH) to reduce the opportunity for non-specific adsorption of proteins to the electrode surface. The sample is added, incubated, and washed, leaving behind CRP bound to the aptamer. Next, a secondary HRP enzyme-labeled antibody is added and binds to CRP. TMB substrate is added and oxidized by any HRP present from binding to CRP. The electrochemical reduction of oxTMB results in a signal proportional to the concentration of CRP in the sample. While this aptasensor enables measurements of CRP, it still requires the same manual steps and trained personnel needed for a traditional immunoassay.

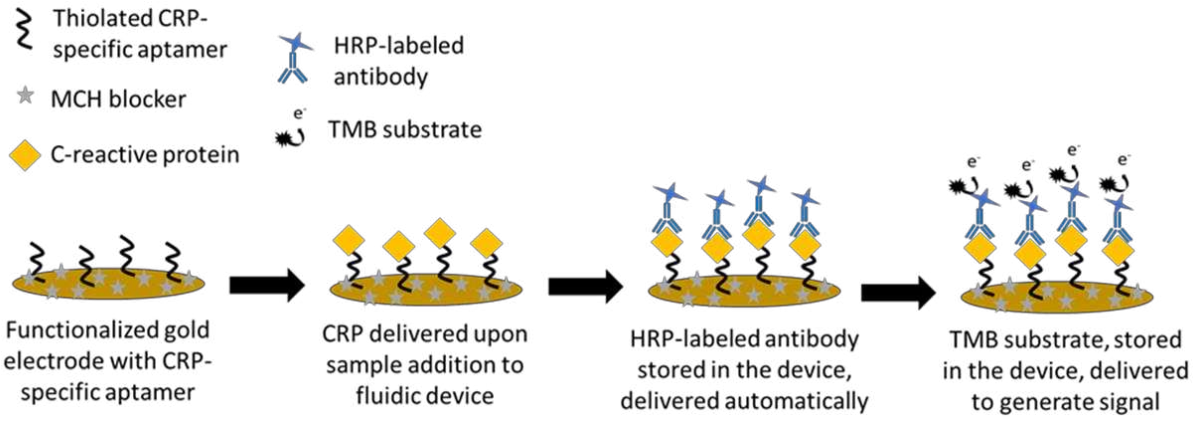

Figure 3.1: Schematic illustrating the functionalization of screen-printed gold electrode with CRP-specific aptamer and subsequent assay steps for electrochemical detection of CRP

Electrochemical detection of CRP: To show the feasibility for CRP measurements, the assay was performed using traditional incubation steps and washes with unoptimized parameters. For this study, 15 µL of 1 nM thiol-terminated aptamer solution was treated with TCEP for 2 hours to reduce disulfide bonds, then heat shocked to ensure proper aptamer folding, and incubated on gold electrodes at 4°C overnight (16 hours). The aptamer solution was removed, and electrodes were washed with PBS, then blocked with 100 µL of 1 mM MCH in PBS for 60 minutes. The MCH solution was removed, electrodes were washed and a 100 µL sample of 10 µg/mL CRP in CRP binding buffer or a blank sample of CRP binding buffer was dropped and incubated for 30 minutes. After removing the solution and washing, 100 µL of 1µg/mL anti-CRP-HRP in antibody binding buffer was dropped and incubated for 30 minutes. This solution was removed, electrodes were washed, and CRP binding buffer was added until measurements could be taken. **Figure 3.2** shows a large difference in current for the 10 µg/mL sample compared to the blank. The average change in current (ΔI) from the blank over a 10 second interval centered at t=60 s was 5.90 ± 1.06 µA. This data validated the ability of the electrodes to detect CRP in buffer. It is important to note the large standard deviation in the 10 µg/mL signal compared to the blank signal. This could be attributed to the lack of a well to contain the solutions added to the electrodes, resulting in variable coverage, or to inadequate washing steps.

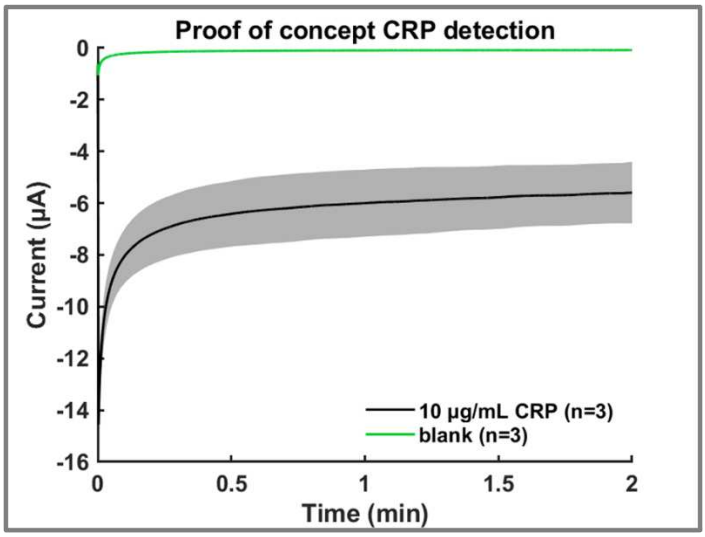

Figure 3.2: Amperometry data collected over 120 seconds from assays performed with blank buffer samples (green) and samples containing 10 µg/mL CRP (black). The lines and shading represent the mean and standard deviation, respectively, of triplicate samples.

Evaluation of assay concentration dependence: To evaluate the performance of the assay spanning the clinical ranges of CRP in both saliva and serum, CRP samples at 1, 10, and 100 ng/mL and 1 and 10 µg/mL were measured using the same parameters as previously described. **Figure 3.3A** shows representative resulting amperograms for each concentration tested. **Figure 3.3B** plots the average change in signal (ΔI) from the blank for triplicate measurements, averaged over a 10 s interval centered at t=60 s. The data is fit to a 4-parameter logistic (4-PL) curve, which is common for these types of assays, [50, 51] and the LOD calculated from the blank signal plus three times the standard deviation of the blank is 79 ng/mL. It is important to note the drastic reduction in signal for this experiment compared to the last. This is likely due to degradation and denaturation of the secondary antibody due to long-term storage. Regardless, there was a distinct increase in signal (Δ)I with each increasing CRP concentration, with the exception of the 10 µg/mL signal, which is slightly lower than the 1 µg/mL. This trend is known as the Hook effect, where an over-

abundance of target analyte begins to shut off signal due to over-crowding of proteins preventing binding of the secondary antibody and electron transfer at the electrode surface. This is common in immunoassays[52] and has also been reported in aptamer-based assays,[53] although some studies have shown methods to prevent the Hook effect in aptasensors through different modification techniques.[54] There is also a significant increase in signal variability at higher concentrations. This could be attributed to differences in electrode coverage that may be improved by reducing the area of the working electrode. Considering that this aptasensor seems to perform better at lower concentrations is a promising attribute for measurements in saliva samples.

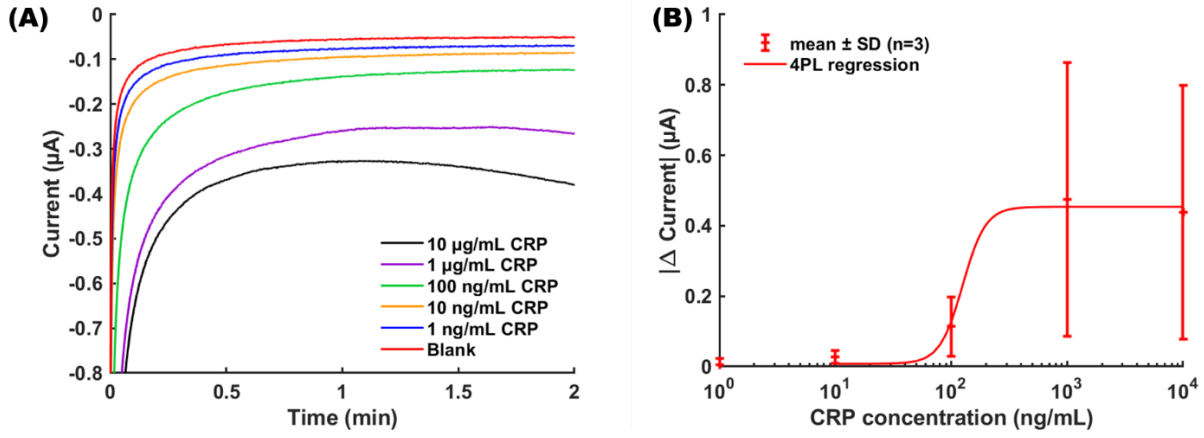

Figure 3.3: (A) Representative amperomery data measured over 120 seconds for triplicate measurements of CRP at concentrations of 1, 10, and 100 ng/mL and 1 and 10 µg/mL. (B) The average change in signal (ΔI) as a function of CRP concentration fit to a 4-parameter logistic (4-PL) curve.

Fluidic device for automation of CRP assay: To improve the accessibility of the assay, the aptasensor was incorporated into a capillary driven device that would automate the assay steps. **Figure 3.4A** shows the alternating layers of PET films (grey) and DSA (green) that were patterned using a CO_2 laser and sandwiched together to create hollow fluidic channels. **Figure 3.4B** illustrates the 3D channels of varying depths that were created using the PET films and DSA and shows the incorporation of conjugate release pads (orange) for drying and storing of reagents

within the device. Glass fiber conjugate release pads containing the enzyme-labeled antibody and substrate were placed withing the channels, so all necessary assay reagents were stored within the device. **Figure 3.4C** shows the assembled device at varying time points after sample addition. The functionalized electrode was added by simply placing it in the template within the cover layer and pressing to seal to the exposed DSA. Finally, a 25 mm Whatman 4 chromatography paper fan was added to the outlet of the device to serve as a passive, capillary-driven pump. **Figure 3.4C(i)** shows the addition of the sample through the inlet of the device. This is the only step required by an end user. **Figure 3.4C(ii)** shows the delivery of the secondary antibody (dried in the yellow conjugate release pad) across the electrode surface. **Figure 3.4C(iii)** shows the delivery of the TMB substrate (dried in the blue conjugate release pad across the electrode). **Figure 3.4D** illustrates the expected amperogram from the assay, represented as a peak as the TMB substrate flows across the electrode surface, producing a change in current.

Similar devices used for previous studies[35] did not allow for the incorporation of commercial electrodes, took about 30 minutes to achieve results, and were prone to device malfunctions. To address these frustrations, a novel fluidic device was created. A series of vents in the cover layer over the channels just below the conjugate release pads assisted in preventing bubbles in the channels that had previously hindered and stopped flow. A larger waste pad, made of a more absorbent filter paper helped to increase flow rates. Finally, the shape of the outlet channel was adapted to create a bubble design. This allowed for complete coverage of solution over the commercial working electrode, helped prevent leaking, and helped increase flow rate compared to the same device design with a straight channel outlet.

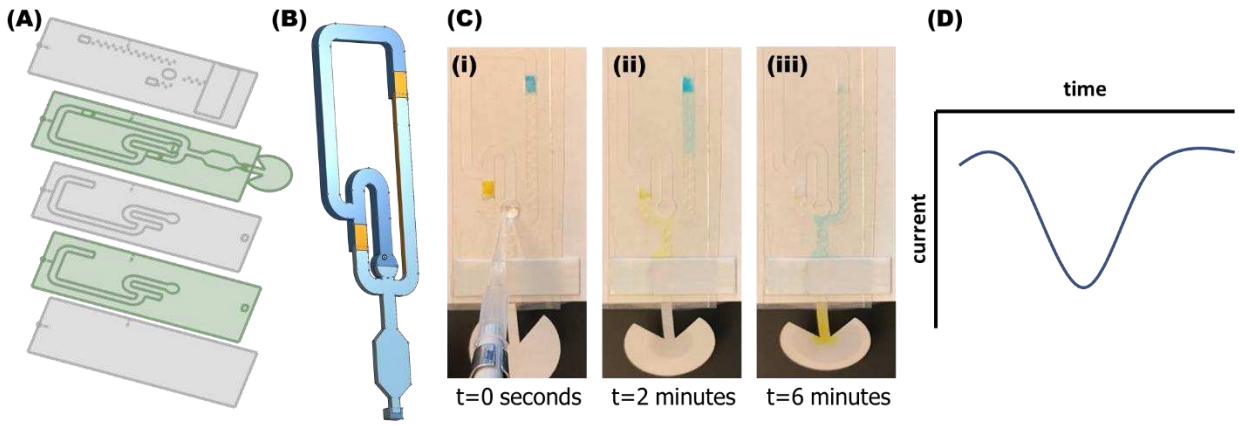

Figure 3.4: (A) Alternating layers of PET film (grey) and DSA (green) that are sandwiched together to create fluidic device. (B) 3-dimensional drawing of hollow channels. (C) Fluidic device at varying time points showing the addition of sample and automated delivery of reagents. (D) Expected amperometric data to be recorded as TMB flows across the electrode.

Adapting assay for compatibility with fluidic device: Transitioning to a fluidic system with the reagents and wash steps delivered automatically requires several changes to the procedure including eliminating the separate buffers needed for the CRP and HRP binding, adding surfactant to the buffer to help with flow through the device, and adding H_2O_2 to catalyze the substrate turnover since the H_2O_2 present in the commercial TMB will not be present once the reagent is dried in the conjugate release pad. Static assay controls and optimization experiments were performed to evaluate the feasibility of transitioning to the fluidic system. In Experiment 1, the effect of a stronger washing step after the blocking for non-specific adsorption was explored. The control experiment consisted of 3 aliquots of 150 µL added to the electrode then removed. To reduce standard deviation, a stronger wash step using spray bottles of TrisT followed by CRP binding buffer were used to wash the electrodes. The addition of surfactant, combined with the force of a spray bottle compared to a pipette, presumably helps remove unbound reagent from the surface. As seen in **Figure 3.5,** Experiment 1, this reduced both the change in signal from the blank (ΔI) and the standard deviation. The stronger washing step was implemented for future

experiments due to the improved reproducibility. In the second experiment, changes in buffers were evaluated with the intent of using the same buffer for both CRP and HRP-antibody binding. The control experiment used the separate buffers used in **Figure 3.5,** The second point added a surfactant, Tween 80, to the CRP binding buffer, but did not change the antibody binding buffer. The third condition removed the BSA from the antibody binding buffer and used the original CRP binding buffer. **Figure 3.5,** Experiment 2 shows the highest ΔI for the surfactant in the CRP binding buffer, but with an increase in error. It is important to note the low ΔI and very large error bars when BSA was left out of the antibody binding buffer. This condition resulted in large variable current in both the target and the blanks, most likely caused by non-specific adsorption of the HRP-antibody to the gold electrode, which is typically prevented with the BSA. Considering this result, it is crucial for the fluidic device to incorporate BSA to help with this binding step. While the cause of the large decrease in ΔI from Experiment 1 to Experiment 2 is not known, we speculate some degradation of the HRP labeled antibody causing the variability in signal.

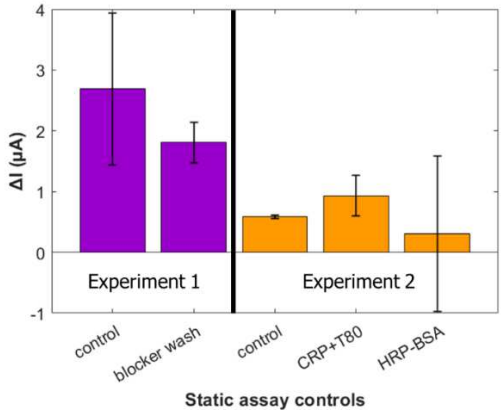

Figure 3.5: Change in current (ΔI) calculated from triplicate samples of 10 μg/mL CRP under varying control conditions. Experiment 1 (purple) compares a blocker wash step using TrisT and CRP binding buffer to a control wash step using only buffer. Experiment 2 compares the control conditions for CRP binding buffer and HRP antibody binding buffer to a condition in which Tween 80 is added to the CRP binding buffer and where BSA is removed from the HRP antibody binding buffer.

Fluidic detection of CRP using eCaDI 2.0: Initial fluidic experiments were performed comparing signal from blank samples and 10 µg/mL CRP samples, with BSA incorporated in the conjugate release pads vs. in the sample buffer. To add BSA to the HRP conjugate release pad, 0.5% BSA was added to the drying buffer. For the BSA in buffer, 0.5% BSA was added to the sample buffer, to make a buffer that consisted of CRP binding buffer with 0.1% Tween 80 and 0.5% BSA. Sample buffer also contained 0.02% H_2O_2 to enable turnover of the substrate. 100 µL of sample was added to the inlet of each device to initiate flow. Amperometric measurements were taken from about 5 minutes after sample addition and ended at 10 minutes after sample addition, resulting in a total run time of 10 minutes, a vast improvement over previous work.[35] **Figure 3.6A** shows the amperometric signal from two blank samples (black) and three samples containing 10 µg/mL CRP (purple). These devices had BSA added to the antibody drying buffer and dried in the pads. **Figure 3.6B** shows the signal for three blank samples (green) and two 10 µg/mL samples (orange) with the 0.5% BSA added to the sample buffer. While there is not a distinct visual difference in the raw data, analysis of averages for both the change in peak area (**Figure 3.6C**) and peak height (**Figure 3.6D)** revealed an increase in signal from blank to target, with better reproducibility with the BSA in the sample buffer. It is important to note the variation in peak shape for many of the devices run. Some exhibit the expected single peak. While others have a clearly pronounced double peak. This is likely caused by changes in fluid dynamics of the device due to manual assembly and placement of the electrode. We also speculate a significant amount of enzyme-substrate turnover occurring within the device channels, as opposed to at the electrode surface. Further optimization is needed to decrease signal from the blank, improve reproducibility, and minimize variation in peak shape.

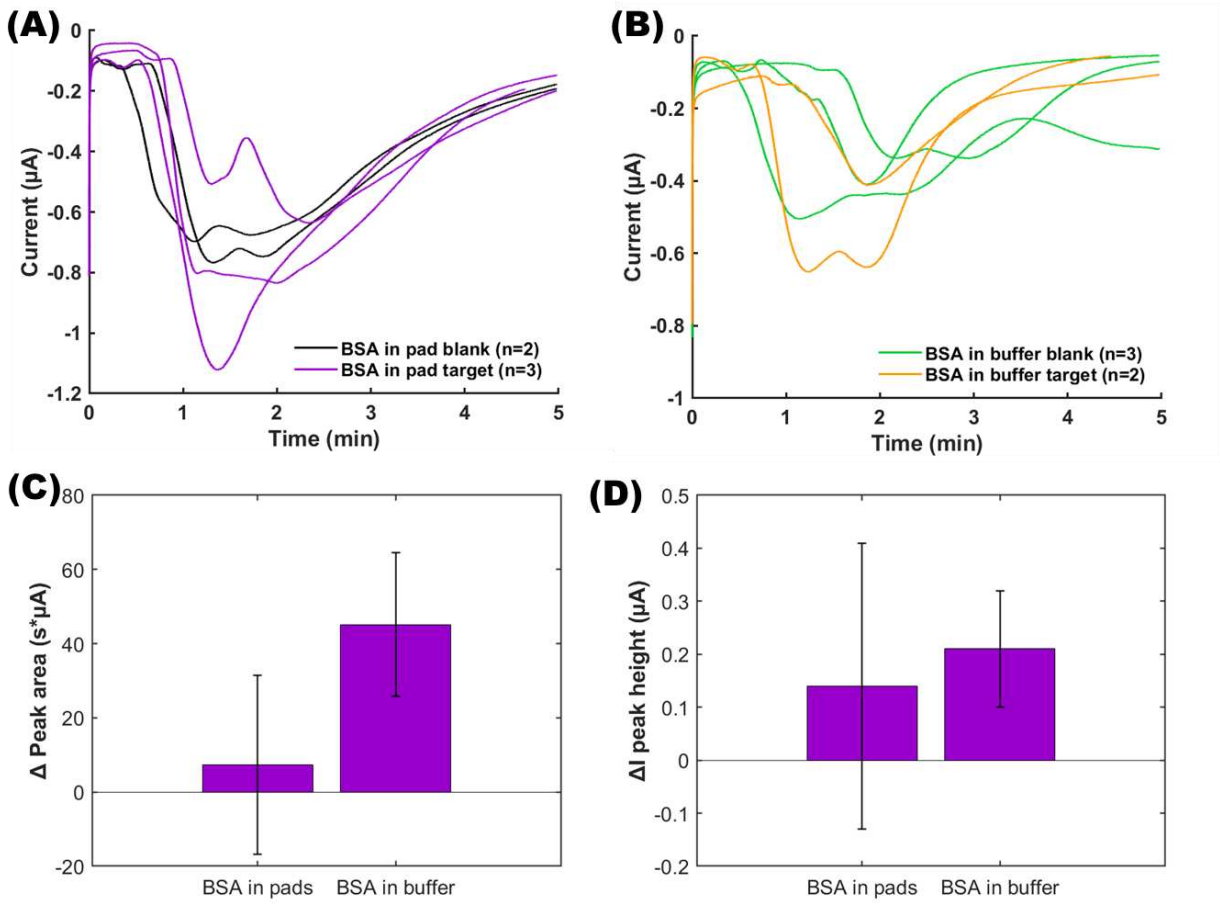

Figure 3.6: (A) Amperometry data collected for blank (black) and 10 µg/mL CRP (purple) samples using the fluidic device with BSA added to the HRP antibody conjugate release pad. (B) Amperometry data collected for blank (green) and 10 µg/mL CRP (orange) samples using the fluidic device with BSA added to the sample buffer. (C) Average change in peak height from the blank for n=3 target sample and n=2 blank samples with BSA in conjugate release pads and n= 2 target and n=3 blank for samples with BSA in buffer. (D) Average change in peak area from the blank for n=3 target sample and n=2 blank samples with BSA in conjugate release pads and n= 2 target and n=3 blank for samples with BSA in buffer.

Evaluation of non-specific interaction of HRP antibody and TMB within device channels: A control experiment was performed to evaluate the amount of enzyme-substrate interaction that was happening within the device channels as opposed to at the electrode surface. For this experiment, a blocked electrode without aptamer on the surface was used in the fluidic device. Blank buffer samples were run with devices containing HRP antibody and TMB substrate and compared to

devices with only TMB substrate. **Figure 3.7** shows the amperograms obtained. There is a clear increase in signal for the devices with both enzyme and substrate (black) compared to the devices with only substrate (purple). This indicates a large amount of enzyme-substrate interaction occurring within the device and can explain the high signal for blanks in previous experiments. To address this issue, further device optimizations need to be made to increase the time of washing steps between reagent delivery and reduce the opportunity for substrate turnover outside of what occurs at the electrode in response to the assay.

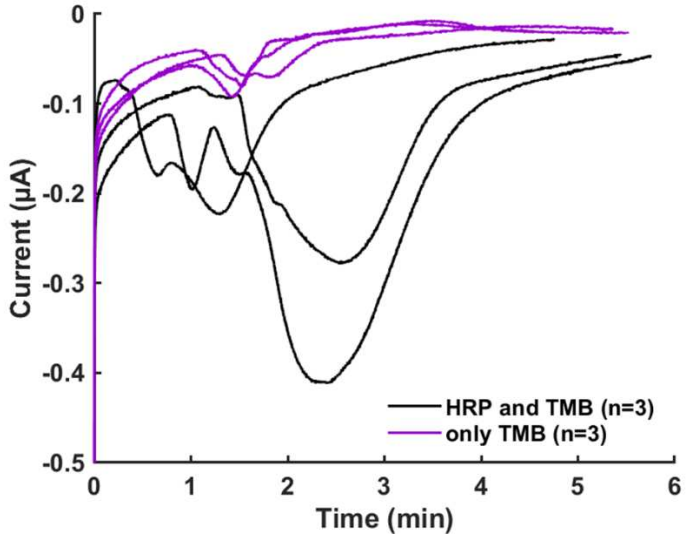

Figure 3.7: Amperometry data comparing the signal from a blank sample in a device without HRP antibody (purple) (n=3) with a device containing HRP antibody and TMB substrate (black) (n=3).

Schematic of carbon electrode aptasensor: Carbon composite electrodes are a lower cost alternative compared to gold electrodes.[55] This makes them appealing for point of care biosensing from a cost standpoint, but they often lack the sensitivity of gold electrodes. To compare the performance of carbon electrodes to gold electrodes, the assay was adjusted for detection using stencil-printed carbon electrodes. Adjustments that were made are illustrated in **Figure 3.8**. The first, and most obvious is the electrode. House-made stencil-printed electrodes were fabricated

using graphite and carbon ink, on PET films. Amine-terminated aptamer of the same nucleic acid sequence was immobilized on the carbon surface via EDC/NHS coupling. Finally, 0.5% ethanolamine was used to block the surface to prevent non-specific adsorption. The subsequent assay steps were unchanged.

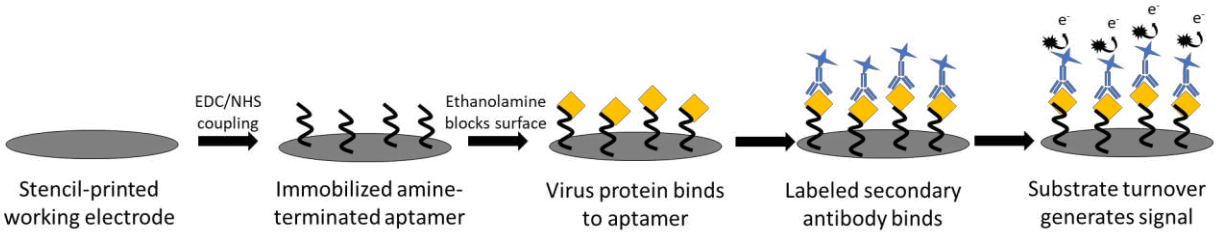

Figure 3.8: Schematic illustrating the assay using stencil-printed carbon electrodes with amine-terminated aptamer immobilized via EDC/NHS coupling and blocked with 0.5% ethanolamine. Subsequent assay steps mirror the assay steps used previously on gold electrodes.

Evaluation of assay performance of carbon electrodes: To evaluate assay performance using carbon electrodes, measurements were taken for triplicate samples of 10 and 100 ng/mL and 1, 10, and 100 µg/mL CRP. **Figure 3.9A** shows the resulting amperograms, and **Figure 3.9B** plots the average change in signal from the blank (ΔI) calculated by averaging current over a 10 s interval centered at t=60 s. There is a clear increase in signal with each of the first 3 concentrations, followed by a significant decrease in signal for the 10 and 100 µg/mL samples. This is likely due to over-crowding of proteins, preventing reduction of TMB at the electrode surface. This is known as the Hook effect and has been observed in both immunoassays[52] and aptamer-based assays. [53] A line of best fit and LOD for this assay could not be calculated because there were not enough points within the dynamic range of the device.

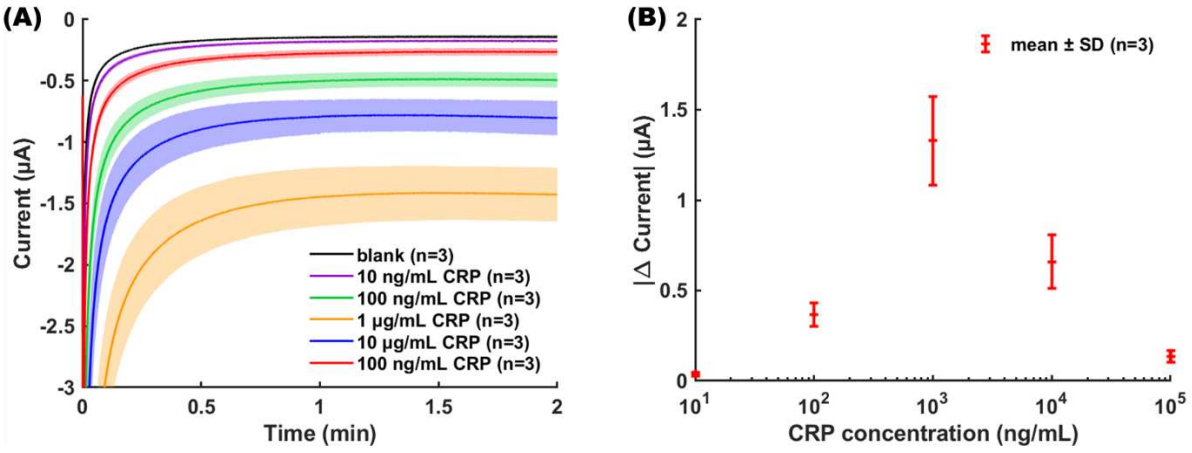

Figure 3.9: (A) Amperomery data measured over 120 seconds for triplicate measurements of CRP at concentrations of 10 and 100 ng/mL, and 1, 10, and 100 µg/mL. The mean and standard deviations of triplicate measurements are represented by the line and shading, respectively. (B) The average change in signal (ΔI) as a function of CRP concentration with error bars representing the standard deviation of triplicates. Acknowledgement: This data was collected by Alli Dolence

Conclusions and Future Directions:

This project is ongoing. Future work before publication includes continued optimization of the fluidic device to reduce the opportunity for enzyme/substrate interaction in the device channels. This can be accomplished by lengthening the channel responsible for the wash step after the HRP antibody delivery, which would likely also increase the sample volume needed. Further optimization of the assay procedure will include buffer optimization, optimization of HRP antibody concentration, and blocker optimization in the hopes of reducing variability between devices. Finally, we will compare the fluidic devices made with carbon electrodes to those with gold electrodes to evaluate the dynamic range of each and determine the viability of a lower-cost device for highly sensitive detection of CRP in saliva.

References

1. Jain, S.; Gautam, V.; Naseem, S., Acute-phase proteins: As diagnostic tool. *Journal of Pharmacy and Bioallied Sciences* **2011,** *3* (1), 118.
2. Desai, G. S.; Mathews, S. T., Saliva as a non-invasive diagnostic tool for inflammation and insulin-resistance. *World journal of diabetes* **2014,** *5* (6), 730.
3. Aguiar, F. J.; Ferreira-Júnior, M.; Sales, M. M.; Cruz-Neto, L. M.; Fonseca, L. A.; Sumita, N. M.; Duarte, N. J.; Lichtenstein, A.; Duarte, A. J., C-reactive protein: clinical applications and proposals for a rational use. *Revista da Associação Médica Brasileira (English Edition)* **2013,** *59* (1), 85-92.
4. Ridker, P. M., Clinical application of C-reactive protein for cardiovascular disease detection and prevention. *Circulation* **2003,** *107* (3), 363-369.
5. Meyer, M. H.; Hartmann, M.; Keusgen, M., SPR-based immunosensor for the CRP detection—A new method to detect a well known protein. *Biosensors and Bioelectronics* **2006,** *21* (10), 1987-1990.
6. Meyer, M. H.; Hartmann, M.; Krause, H.-J.; Blankenstein, G.; Mueller-Chorus, B.; Oster, J.; Miethe, P.; Keusgen, M., CRP determination based on a novel magnetic biosensor. *Biosensors and bioelectronics* **2007,** *22* (6), 973-979.
7. Kim, C.-H.; Ahn, J.-H.; Kim, J.-Y.; Choi, J.-M.; Lim, K.-C.; Park, T. J.; Heo, N. S.; Lee, H. G.; Kim, J.-W.; Choi, Y.-K., CRP detection from serum for chip-based point-of-care testing system. *Biosensors and Bioelectronics* **2013,** *41*, 322-327.
8. Noh, S.; Kim, J.; Kim, G.; Park, C.; Jang, H.; Lee, M.; Lee, T., Recent advances in CRP biosensor based on electrical, electrochemical and optical methods. *Sensors* **2021,** *21* (9), 3024.
9. Lin, S.-C.; Tseng, C.-Y.; Lai, P.-L.; Hsu, M.-Y.; Chu, S.-Y.; Tseng, F.-G.; Cheng, C.-M., based CRP monitoring devices. *Scientific reports* **2016,** *6* (1), 1-7.
10. Sohrabi, H.; kholafazad Kordasht, H.; Pashazadeh-Panahi, P.; Nezhad-Mokhtari, P.; Hashemzaei, M.; Majidi, M. R.; Mosafer, J.; Oroojalian, F.; Mokhtarzadeh, A.; de la Guardia, M., Recent advances of electrochemical and optical biosensors for detection of C-reactive protein as a major inflammatory biomarker. *Microchemical Journal* **2020,** *158*, 105287.
11. Mahmoudinobar, F.; Britton, D.; Montclare, J. K., Protein-based lateral flow assays for COVID-19 detection. *Protein Engineering, Design and Selection* **2021,** *34*.
12. Ong, D. S.; De Man, S.; Lindeboom, F. A.; Koeleman, J. G., Comparison of diagnostic accuracies of rapid serological tests and ELISA to molecular diagnostics in patients with suspected coronavirus disease 2019 presenting to the hospital. *Clinical Microbiology and Infection* **2020,** *26* (8), 1094. e7-1094. e10.
13. Cheng, J.; Yang, G.; Guo, J.; Liu, S.; Guo, J., Integrated electrochemical lateral flow immunoassays (eLFIAs): recent advances. *Analyst* **2022,** *147* (4), 554-570.
14. Lee, K. S.; Kim, T.-H.; Shin, M.-C.; Lee, W.-Y.; Park, J.-K., Disposable liposome immunosensor for theophylline combining an immunochromatographic membrane and a thick-film electrode. *Analytica chimica acta* **1999,** *380* (1), 17-26.
15. Dempsey, E.; Rathod, D., Disposable printed lateral flow electrochemical immunosensors for human cardiac troponin T. *IEEE Sensors Journal* **2018,** *18* (5), 1828-1834.
16. Inoue, K.; Ferrante, P.; Hirano, Y.; Yasukawa, T.; Shiku, H.; Matsue, T., A competitive immunochromatographic assay for testosterone based on electrochemical detection. *Talanta* **2007,** *73* (5), 886-892.

17. Akanda, M. R.; Joung, H.-A.; Tamilavan, V.; Park, S.; Kim, S.; Hyun, M. H.; Kim, M.-G.; Yang, H., An interference-free and rapid electrochemical lateral-flow immunoassay for one-step ultrasensitive detection with serum. *Analyst* **2014,** *139* (6), 1420-1425.
18. Yasukawa, T.; Kiba, Y.; Mizutani, F., A dual electrochemical sensor based on a test-strip assay for the quantitative determination of albumin and creatinine. *Analytical Sciences* **2015,** *31* (7), 583-589.
19. Bhardwaj, J.; Sharma, A.; Jang, J., Vertical flow-based paper immunosensor for rapid electrochemical and colorimetric detection of influenza virus using a different pore size sample pad. *Biosensors and Bioelectronics* **2019,** *126*, 36-43.
20. Chen, X.; Dong, T.; Wei, X.; Yang, Z.; Pires, N. M. M.; Ren, J.; Jiang, Z., Electrochemical methods for detection of biomarkers of Chronic Obstructive Pulmonary Disease in serum and saliva. *Biosensors and Bioelectronics* **2019,** *142*, 111453.
21. Pfaffe, T.; Cooper-White, J.; Beyerlein, P.; Kostner, K.; Punyadeera, C., Diagnostic potential of saliva: current state and future applications. *Clinical chemistry* **2011,** *57* (5), 675-687.
22. Zheng, X.; Zhang, F.; Wang, K.; Zhang, W.; Li, Y.; Sun, Y.; Sun, X.; Li, C.; Dong, B.; Wang, L., Smart biosensors and intelligent devices for salivary biomarker detection. *TrAC Trends in Analytical Chemistry* **2021,** *140*, 116281.
23. Dillon, M. C.; Opris, D. C.; Kopanczyk, R.; Lickliter, J.; Cornwell, H. N.; Bridges, E. G.; Nazar, A. M.; Bridges, K. G., Detection of homocysteine and C-reactive protein in the saliva of healthy adults: comparison with blood levels. *Biomarker insights* **2010,** *5*, BMI. S5305.
24. Mirzaii-Dizgah, I.; Riahi, E.; Miri, R., Serum and saliva levels of high-sensitivity C-reactive protein in acute myocardial infarction. *J Mol Biomark Diagn* **2012,** *3* (4), 128-132.
25. Ouellet-Morin, I.; Danese, A.; Williams, B.; Arseneault, L., Validation of a high-sensitivity assay for C-reactive protein in human saliva. *Brain, Behavior, and Immunity* **2011,** *25* (4), 640-646.
26. Punyadeera, C.; Dimeski, G.; Kostner, K.; Beyerlein, P.; Cooper-White, J., One-step homogeneous C-reactive protein assay for saliva. *Journal of immunological methods* **2011,** *373* (1-2), 19-25.
27. Mohamed, R.; Campbell, J.-L.; Cooper-White, J.; Dimeski, G.; Punyadeera, C., The impact of saliva collection and processing methods on CRP, IgE, and Myoglobin immunoassays. *Clinical and translational medicine* **2012,** *1* (1), 1-8.
28. Labat, C.; Temmar, M.; Nagy, E.; Bean, K.; Brink, C.; Benetos, A.; Bäck, M., Inflammatory mediators in saliva associated with arterial stiffness and subclinical atherosclerosis. *Journal of hypertension* **2013,** *31* (11), 2251.
29. Pay, J. B.; Shaw, A. M., Towards salivary C-reactive protein as a viable biomarker of systemic inflammation. *Clinical biochemistry* **2019,** *68*, 1-8.
30. Lee, S. H.; Choi, S.; Kwon, K.; Bae, N.-H.; Kwak, B. S.; Cho, W. C.; Lee, S. J.; Jung, H.-I., A photothermal biosensor for detection of C-reactive protein in human saliva. *Sensors and Actuators B: Chemical* **2017,** *246*, 471-476.
31. Hu, W.; Dang, T.; Li, Z.; Lei, L.; Wang, G.; Li, Y.; Xu, H.; Zhou, Z.; Liu, G. L., C-reaction protein detection in human saliva by nanoplasmonic color imaging. *Journal of Biomedical Nanotechnology* **2019,** *15* (8), 1724-1733.
32. Petruzzi, L.; Maier, T.; Ertl, P.; Hainberger, R., Quantitative detection of C-reactive protein in human saliva using an electrochemical lateral flow device. *Biosensors and Bioelectronics: X* **2022,** *10*, 100136.

33. Jang, I.; Kang, H.; Song, S.; Dandy, D. S.; Geiss, B. J.; Henry, C. S., Flow control in a laminate capillary-driven microfluidic device. *Analyst* **2021,** *146* (6), 1932-1939.
34. Carrell, C.; Link, J.; Jang, I.; Terry, J.; Scherman, M.; Call, Z.; Panraksa, Y.; Dandy, D. S.; Geiss, B. J.; Henry, C., Point-of-Need Disposable ELISA System for COVID-19 Serology Testing. **2020**.
35. Kaylee M. Clark, M. S. S., Trey W. Pittman, Isabelle C. Samper, Loran BR Anderson, Wisarut Khamcharoen, Suad Elmergerhi, Rushika Perera, Alan J. Kennan, Brian J. Geiss, David S. Dandy, and Charles S. Henry, Electrochemical Capillary Driven Immunoassay for Detection of SARS-CoV-2. *ACS Measurement Science Au (accepted)* **2022**.
36. Samper, I. C.; McMahon, C. J.; Schenkel, M. S.; Clark, K. M.; Khamcharoen, W.; Anderson, L. B.; Terry, J. S.; Gallichotte, E. N.; Ebel, G. D.; Geiss, B. J., Electrochemical Immunoassay for the Detection of SARS-CoV-2 Nucleocapsid Protein in Nasopharyngeal Samples. *Analytical chemistry* **2022,** *94* (11), 4712-4719.
37. Zhou, W.; Huang, P.-J. J.; Ding, J.; Liu, J., Aptamer-based biosensors for biomedical diagnostics. *Analyst* **2014,** *139* (11), 2627-2640.
38. Ling, K.; Jiang, H.; Zhang, L.; Li, Y.; Yang, L.; Qiu, C.; Li, F.-R., A self-assembling RNA aptamer-based nanoparticle sensor for fluorometric detection of Neomycin B in milk. *Analytical and bioanalytical chemistry* **2016,** *408* (13), 3593-3600.
39. Han, K.; Liang, Z.; Zhou, N., Design strategies for aptamer-based biosensors. *Sensors* **2010,** *10* (5), 4541-4557.
40. Bini, A.; Centi, S.; Tombelli, S.; Minunni, M.; Mascini, M., Development of an optical RNA-based aptasensor for C-reactive protein. *Analytical and Bioanalytical Chemistry* **2008,** *390* (4), 1077-1086.
41. Vance, S. A.; Sandros, M. G., Zeptomole detection of C-reactive protein in serum by a nanoparticle amplified surface plasmon resonance imaging aptasensor. *Scientific reports* **2014,** *4* (1), 1-7.
42. Wang, J.; Guo, J.; Zhang, J.; Zhang, W.; Zhang, Y., RNA aptamer-based electrochemical aptasensor for C-reactive protein detection using functionalized silica microspheres as immunoprobes. *Biosensors and Bioelectronics* **2017,** *95*, 100-105.
43. Jarczewska, M.; Rębiś, J.; Górski, Ł.; Malinowska, E., Development of DNA aptamer-based sensor for electrochemical detection of C-reactive protein. *Talanta* **2018,** *189*, 45-54.
44. Chen, X.; Liu, X.; Zhang, C.; Meng, H.; Liu, B.; Wei, X., A rapid fluorescent aptasensor for point-of-care detection of C-reactive protein. *Talanta* **2022**, 123661.
45. Pultar, J.; Sauer, U.; Domnanich, P.; Preininger, C., Aptamer–antibody on-chip sandwich immunoassay for detection of CRP in spiked serum. *Biosensors and Bioelectronics* **2009,** *24* (5), 1456-1461.
46. Bernard, E. D.; Nguyen, K. C.; DeRosa, M. C.; Tayabali, A. F.; Aranda-Rodriguez, R., Development of a bead-based aptamer/antibody detection system for C-reactive protein. *Analytical biochemistry* **2015,** *472*, 67-74.
47. Technologies, I. D. Reduction for Oligonucleotides with thiol modifications.
48. Jayasena, S. D., Aptamers: an emerging class of molecules that rival antibodies in diagnostics. *Clinical chemistry* **1999,** *45* (9), 1628-1650.
49. Torres-Chavolla, E.; Alocilja, E. C., Aptasensors for detection of microbial and viral pathogens. *Biosensors and bioelectronics* **2009,** *24* (11), 3175-3182.

50. O'Connell, M.; Belanger, B.; Haaland, P., Calibration and assay development using the four-parameter logistic model. *Chemometrics and Intelligent Laboratory Systems* **1993,** *20* (2), 97-114.
51. Heineman, W. R.; Halsall, H. B., Strategies for electrochemical immunoassay. *Analytical chemistry* **1985,** *57* (12), 1321A-1331A.
52. Hoofnagle, A. N.; Wener, M. H., The fundamental flaws of immunoassays and potential solutions using tandem mass spectrometry. *Journal of immunological methods* **2009,** *347* (1-2), 3-11.
53. Long, Y.; Ai, Z.; Zhang, L.; Zhang, H.; Jiang, J.; Liu, G. L., Low-Cost, High Sensitivity Paper-Based Bacteria Impedance Sensor Based on Vertical Flow Assay. *High Sensitivity Paper-Based Bacteria Impedance Sensor Based on Vertical Flow Assay*.
54. Cass, A. E.; Zhang, Y., Nucleic acid aptamers: ideal reagents for point-of-care diagnostics? *Faraday discussions* **2011,** *149* (1), 49-61.
55. McCreery, R. L., Advanced carbon electrode materials for molecular electrochemistry. *Chemical reviews* **2008,** *108* (7), 2646-2687.

Chapter 4: Conclusions and future directions

The Covid-19 pandemic shed light on the already evident need for improvements in diagnostics, especially at the point of care. Existing gold standards for diagnostics like reverse transcriptase polymerase chain reaction (rt-PCR) and immunoassays need to be performed by trained personnel in a laboratory setting, can be time consuming, and require expensive instrumentation. This drives up the cost and limits the number of tests that can be run, resulting in overwhelmed laboratories, especially during crises like the COVID-19 pandemic.[1]

Alternative diagnostic approaches, like lateral flow assays (LFAs) provide a diagnostic platform that is available at the point of care. A single sample addition step, performed by the end user, can result in a positive or negative readout.[2] Despite the simplicity and ease of use, these devices typically suffer from low sensitivity and poor limits of detection.[3, 4]

A new class of fluidic devices, introduced by the Henry group, creates hollow channels through alternating layers of patterned polyethylene terephthalate (PET) films and double-sided adhesives (DSA).[5, 6] These devices are capable of controlling flow such that sequential delivery of reagents can be accomplished.[7] Further, the incorporation of electrochemical biosensors with the capillary-driven fluidic devices provides a platform that can provide the ease of use of an LFA, with the high sensitivity, specificity, and quantitative results provided by electrochemical biosensors.

The work presented in **Chapter 2** of this dissertation describes an electrochemical immunosensor developed for highly sensitive detection of Covid-19 N-Protein.[8] The work goes on to adapt the method for compatibility with a capillary-driven immunoassay device to accomplish detection after a single sample addition.[9] The assay is optimized for compatibility

with the device, and functionalization of the electrodes is optimized for manufacturing-friendly procedures. Finally, the fluidic device, with incorporated electrodes, demonstrated concentration-dependent signal for samples containing SARS-CoV-2 inactivated virus. While this work served as a proof-of-concept for automated assays with electrochemical detection, more work is needed to improve limits of detection, accomplish device compatibility with clinical samples, reduce time to result, and improve device fabrication procedures. We reported an impressive 7+ weeks of stability for the functionalized electrodes, but the reagent pads for the device were not tested for stability and are not likely stable for long periods of time. Further studies are needed to improve reagent stability in the conjugate release pads and evaluate best storage conditions for the assembled device. Previous studies have explored the ability of commercial stabilizers to preserve immunogenic activity,[10] and evaluated different additives to improve storage of antibodies in paper.[11] It is likely that these previous studies will provide valuable insight into improving storage of the enzyme-labeled antibody pad. The TMB substrate also presents issues, since it is prone to light-induced auto-oxidation.[12] This can be easily addressed with appropriate packaging. If other stability issues arise, other enzyme-substrate pairs could be explored.

Chapter 3 of this report is a continuation of the fluidic device presented in **Chapter 2**. The device design was modified for compatibility with commercial electrodes, to increase flow rate and reduce time to result, and to decrease opportunities for device malfunctions. The electrochemical biosensor incorporated in this device made use of highly sensitive screen-printed gold electrodes, and CRP-specific aptamers as biorecognition elements. This was done to increase sensitivity, which is needed for CRP measurements in saliva samples. Immediate future work on this device includes CRP assay optimizations to improve reproducibility and sensitivity,

and to extend the linear range. Device modifications are still needed to reduce non-specific signal from the enzyme-substrate reaction within the device.

Overall, this work serves as a stepping stone toward more sensitive, user-friendly diagnostic options. While further optimizations are needed before this device could be useful in commercial applications, this is the first step in enabling highly sensitive electrochemical detection of biological analytes with the ease of use of an LFA.

Future directions:

Going forward, electrochemical capillary-driven fluidic devices can continue to be developed for existing and emerging viruses, proteins, antibodies, etc. Taking advantage of the widespread applications of aptamers, similar assays could also be developed for metal ions, small molecules like amino acids, antibiotics, and vitamins, and even bacteria.[13] Extending the diagnostic and detection options available at the point of care will have a positive impact on overall human health.

In continuing to develop and optimize the fluidic platform, one future goal includes multiplexing the device for simultaneous detection of multiple analytes. A recent publication by Shu *et al.* reported a multiplex rt-PCR test for Influenza A and B, and SARS-CoV-2 to reduce the strain on current testing facilities.[14] The ability to make this type of test available at the point of care would further reduce the strain on testing facilities and also provide end users with faster readouts. Multiplexing of the electrochemical capillary-driven assay could be accomplished through manipulation of channels to flow independently across two or more electrode systems integrated within the device. Eventually, various biomarkers can be explored for more wholistic diagnostic options.

In summary, this dissertation reports developments in electrochemical point of care diagnostic devices. By incorporating electrochemical biosensors into capillary-driven fluidic devices, a novel diagnostic platform was created. This system has the potential to provide the highly sensitive and specific detection that is typically seen in sophisticated laboratory procedures with the ease of use of a lateral flow assay. Work here focused on detection of SARS-CoV-2 N-protein and C-reactive protein, although the system could be applied to a wide range of analytes. These types of developments in diagnostic technologies pave the way to improve overall human health.

References

1. Motley, M. P.; Bennett-Guerrero, E.; Fries, B. C.; Spitzer, E. D., Review of viral testing (polymerase chain reaction) and antibody/serology testing for severe acute respiratory syndrome-coronavirus-2 for the intensivist. *Critical care explorations* **2020,** *2* (6).
2. Posthuma-Trumpie, G. A.; Korf, J.; van Amerongen, A., Lateral flow (immuno) assay: its strengths, weaknesses, opportunities and threats. A literature survey. *Analytical and bioanalytical chemistry* **2009,** *393* (2), 569-582.
3. Mahmoudinobar, F.; Britton, D.; Montclare, J. K., Protein-based lateral flow assays for COVID-19 detection. *Protein Engineering, Design and Selection* **2021,** *34*.
4. Ong, D. S.; De Man, S.; Lindeboom, F. A.; Koeleman, J. G., Comparison of diagnostic accuracies of rapid serological tests and ELISA to molecular diagnostics in patients with suspected coronavirus disease 2019 presenting to the hospital. *Clinical Microbiology and Infection* **2020,** *26* (8), 1094. e7-1094. e10.
5. Jang, I.; Carrão, D. B.; Menger, R. F.; Moraes de Oliveira, A. R.; Henry, C. S., Pump-free microfluidic rapid mixer combined with a paper-based channel. *ACS sensors* **2020,** *5* (7), 2230-2238.
6. Jang, I.; Kang, H.; Song, S.; Dandy, D. S.; Geiss, B. J.; Henry, C. S., Flow control in a laminate capillary-driven microfluidic device. *Analyst* **2021,** *146* (6), 1932-1939.
7. Carrell, C.; Link, J.; Jang, I.; Terry, J.; Scherman, M.; Call, Z.; Panraksa, Y.; Dandy, D. S.; Geiss, B. J.; Henry, C., Point-of-Need Disposable ELISA System for COVID-19 Serology Testing. **2020**.
8. Samper, I. C.; McMahon, C. J.; Schenkel, M. S.; Clark, K. M.; Khamcharoen, W.; Anderson, L. B.; Terry, J. S.; Gallichotte, E. N.; Ebel, G. D.; Geiss, B. J., Electrochemical Immunoassay for the Detection of SARS-CoV-2 Nucleocapsid Protein in Nasopharyngeal Samples. *Analytical chemistry* **2022,** *94* (11), 4712-4719.
9. Dempsey, E.; Rathod, D., Disposable printed lateral flow electrochemical immunosensors for human cardiac troponin T. *IEEE Sensors Journal* **2018,** *18* (5), 1828-1834.
10. Park, J.-W.; Kurosawa, S.; Aizawa, H.; Wakida, S.-i.; Yamada, S.; Ishihara, K., Comparison of stabilizing effect of stabilizers for immobilized antibodies on QCM immunosensors. *Sensors and Actuators B: Chemical* **2003,** *91* (1-3), 158-162.
11. Guan, L.; Cao, R.; Tian, J.; McLiesh, H.; Garnier, G.; Shen, W., A preliminary study on the stabilization of blood typing antibodies sorbed into paper. *Cellulose* **2014,** *21* (1), 717-727.
12. Liu, Y.; Wang, X.; Wei, H., Light-responsive nanozymes for biosensing. *Analyst* **2020,** *145* (13), 4388-4397.
13. Song, S.; Wang, L.; Li, J.; Fan, C.; Zhao, J., Aptamer-based biosensors. *TrAC Trends in Analytical Chemistry* **2008,** *27* (2), 108-117.
14. Shu, B.; Kirby, M. K.; Davis, W. G.; Warnes, C.; Liddell, J.; Liu, J.; Wu, K.-H.; Hassell, N.; Benitez, A. J.; Wilson, M. M., Multiplex real-time reverse transcription PCR for influenza A virus, influenza B virus, and severe acute respiratory syndrome coronavirus 2. *Emerging infectious diseases* **2021,** *27* (7), 1821.